EADS INNOVATION WORKS

International Committee on Aeronautical Fatigue 2013

# Review of Aeronautical Fatigue Investigations in Germany during the Period April 2011 to April 2013

**Dr. Claudio Dalle Donne**
**EADS Innovation Works**
**CTO/IW-MS-2013-069**

EADS

# Review of Aeronautical Fatigue Investigations in Germany during the Period April 2011 to April 2013

Dr. Claudio Dalle Donne
EADS Innovation Works
CTO/IW-MS

CTO/IW-MS-2013-069 Technical Report
EADS Innovation Works

Title

# Review of Aeronautical Fatigue Investigations in Germany during the Period April 2011 to April 2013

Author
Dr. Claudio Dalle Donne

Project-No.

| Phone | Department/Work area | Date | Report-Nr. |
|---|---|---|---|
| +49-89.607 27728 | CTO/IW-MS | April 2013 | CTO/IW-MS-2013-069 |

Abstract

This review embodies a compilation of abstracts on aeronautical fatigue investigations in Germany during the period April 2011 to April 2013 and is presented within the scope of the Meeting of the International Committee on Aeronautical Fatigue in Jerusalem, Israel, June 3rd-5th 2013.

The contribution of summaries by German aerospace manufacturers, governmental and private research institutes, universities as well as aerospace authorities was completely voluntary, and is acknowledged with sincere appreciation by the authors of this review.

Enquiries concerning the contents should be addressed directly to the author of the corresponding summary.

Distribution to

CTO/IW-OP-IP-Patents (e-mail to Mrs. Rotter)
M&W Zander / KD – Dokumentenverarbeitung/Mikrofilm
Coverpage: CTO/IW – Yann Barbaux, CTO/IW-MG – Mr. Lindemann (via e-mail in pdf. format)

| pages | photos | drawings | diagrams | tables |
|---|---|---|---|---|
| 57 | 16 | 10 | 45 | 1 |

Keywords for database
International Committee on Aeronautical Fatigue, ICAF 2013, National Delegate Review

[1] Classification
1 generally accessible
2 free distribution inside EADS
3 confidential
4 highly confidential

Acceptance

Dr. Claudio Dalle Donne
Head of responsible department

EADS

## Table of contents

# 1 Introduction

This review embodies a compilation of abstracts on aeronautical fatigue investigations in Germany during the period April 2011 to April 2013 and is presented within the scope of the Meeting of the International Committee on Aeronautical Fatigue in Fatigue in Jerusalem, Israel, June 3rd-5th 2013.
The contribution of summaries by German aerospace manufacturers, governmental and private research institutes, universities as well as aerospace authorities was completely voluntary, and is acknowledged with sincere appreciation by the authors of this review.
Enquiries concerning the contents should be addressed directly to the author of the corresponding summary.

### Mailing addresses of contributing companies and institutes:

| Abbreviation | Details |
|---|---|
| Airbus | Airbus Operations GmbH; Kreetslag 10, D-21129 Hamburg, Germany, www.airbus.com |
| AICFS | AICFS – Academic Institute for Creating Fundamental Sciences<br>Westendstr. 68, D-80339 Munich, Germany |
| DLR WF | German Aerospace Center DLR, Institute of Materials Research, Linder Höhe, 51174 Cologne, Germany, www.dlr.de |
| EADS IW | EADS-IW European Aeronautic Defence and Space Company, Innovation Works;<br>D-81663 Munich, Germany, www.eads.net |
| HZG | Helmholtz-Zentrum Geesthacht; Max-Planck-Straße 1,D-21502 Geesthacht, Germany, www.hzg.de |
| IABG | Industrieanlagen-Betriebsgesellschaft mbH; PO-Box 1212, D-85503 Ottobrunn, Germany, www.iabg.de |
| IMA | IMA Materialforschung und Anwendungstechnik GmbH; Postfach 80 01 44, D-01101 Dresden, Germany, www.ima-dresden.de |
| IMR | University of Siegen, Institut für Mechanik und Regelungstechnik;<br>Paul-Bonatz-Strasse 9-11, D-57076 Siegen, Germany, www.uni-siegen.de |
| LMW | University of Siegen, Research Group for Material Science and Material Testing;<br>Paul-Bonatz-Strasse 9-11, D-57076 Siegen, Germany, www.uni-siegen.de |
| RR | Rolls-Royce Deutschland, Eschenweg 11, 15827 Blankenfelde-Mahlow, Germany, www.rolls-royce.com/deutschland/de/ |
| TUD | TU Dresden, Institut für Werkstoffwissenschaft, Helmholtzstr. 7, 01069 Dresden, materials.mw.tu-dresden.de |

# 2 Full Scale Testing

## 2.1 Overview of Full Scale Fatigue Tests (April 2013)

| Project | Customer | Test Structure | Schedule | Laboratory |
|---|---|---|---|---|
| Fuselage Panel Testing | Airbus | Fatigue testing of a new test concept, fatigue test of metal panels | 2011-2012 | IMA |
| Component of High Lift System | XX | Fatigue test using real time load simulation | 2010-2012 | IMA |
| Sonic Fatigue | Airbus | Sonic fatigue test | 2012-2013 | IMA |
| A380 FSFT | Airbus | A380 Full scale fatigue test | 2005-2013 | IABG |
| A380 Skin Panel Fatigue Test | Airbus | VTP structure represented by Flat Panel | 2010 | IMA |
| AgustaWestland AW189 | Liebherr Aerospace | Main Landing Gear, Nose Landing Gear | 2010 - 2014 | IABG |
| Airbus A320 NEF2 ESG | Airbus | Centre fuselage with both wings | 2007 - 2013 | IABG |
| Airbus A350 XWB EW | Airbus | LH Wing | 2013 – 2015 | IABG |
| Airbus A350 XWB EF2 | Airbus | Centre fuselage with both wings | 2013 – 2016 | IABG |
| Airbus A400M EF | Airbus-D | Complete Airframe | 2011 – 2014 | IABG |

**Table 1: Overview of full scale tests; currently running and/or finalised between 2011 and 2013**

## 2.2 A380 EF Full-Scale Fatigue Tests

*W. Göbel (Airbus)*

In September 2012 the fatigue and damage tolerance phase of the A380 Full-Scale Fatigue Test accomplished 3.2 Design Service Goals (60,800 FC). After the Residual Strength Tests in December 2012 the test performance phase was finished. Currently dismantling and tear down investigations are on-going.

A huge number of major and minor findings have been detected during the test. The findings are more or less equally split between wings and fuselage. About 85 % of the findings on Forward and Aft Fuselage Section under Airbus-Germany responsibility occurred in standard aluminium alloys. The remaining 15 % were found on steel, titanium or GLARE® fiber metal laminates.

Additionally a lot of artificial damages have been introduced in order to support the determination or optimisation of the structure maintenance programme thresholds and inspection intervals.

Finally nine residual strength cases were successfully loaded on the structure. No significant damage growth has been detected.

The design and stress teams responsible for the individual work packages have or are still investigating the findings. The investigations comprise(d) design and justification of repairs during the fatigue and damage tolerance phase, determination of modifications for serial aircraft and inspection and modification service bulletins for in-service aircraft. The results will allow an up-

date of the thresholds and intervals of the maintenance program, especially the Airworthiness Limitation Section Part 2 (damage tolerant airworthiness limitation items).

In addition a Parametric Study is performed with 11 different fatigue missions taking real fleet data like range, centre of gravity, payload, fuel at landing, etc. into account.

The investigations are supported by measurements taken at 18,000 measurement channels (single gauges, rosettes). The measurements allow a better correlation of the fatigue life and crack growth prediction based on the theoretical load spectrum and global or detailed local finite element and the load spectrum applied on the test. The effects/constrains of discrete load introduction, hydraulic jack positions, simplification of loading program for test speed optimization are taken into account.

The test proved the good fatigue behaviour of the GLARE® fiber metal laminates skin material applied on fuselage sections 13 and 18. On the other hand the test shows that high strength aluminium alloys require special care during design phase.
Dresden contributes to Full Scale Fatigue Testing of the Airbus A380-800*. The principle task is the provision of test equipment (test hangar, hydraulic and pneumatic hardware) as well as its monitoring and maintenance during testing.
IMA Dresden is also primarily responsible for the regular inspection and Non Destructive Testing (NDT). Used Non-Destructive inspection methods are visual-, eddy-current-, ultra-sonic-, and x-ray inspection.

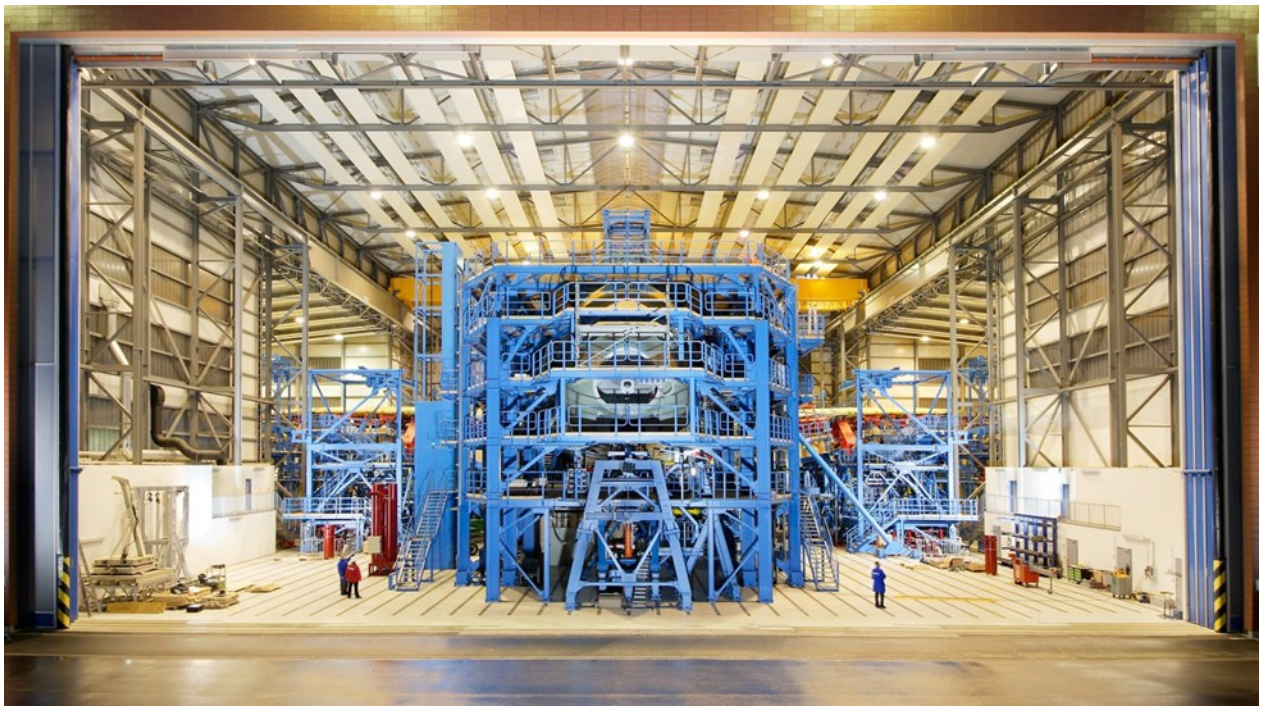

**Figure 2.1 Test Hangar of the A380 EF in Dresden, Germany.**

## 2.3 A350 Full-Scale Fatigue Tests – Status

*W. Göbel (Airbus)*

Currently the full-scale fatigue tests for A350XWB are in preparation Some pre-tests have already been performed with a relatively low load level. These tests form the most upper level of the A350XWB test pyramid (sometimes also called building block approach) supporting Means of Compliance (MoC) for metallic and composite fatigue and damage tolerance together with an ES static test, EW wing box and fuselage barrel composite fatigue and damage tolerance tests.

The fatigue tests are performed in line with the airworthiness rules EASA CS 25.571 and FAA FAR 25.571 (including the new rule for WFD issued Jan. 2011).

The test objective is focused on Metal and Composite Fatigue and Damage Tolerance, i.e. damage initiation and damage propagation.

The tests are representing the primary structure of the airframe, i.e. fuselage and wing. Load introduction dummies representing the landing gears, pylon, movables, horizontal and vertical tail plane (HTP and VTP).

The EF1 consists of cockpit and fwd fuselage sections 11, 12 and partially section 13. Center Fuselage section 15 and center wing box section 21 and a pair of wings are forming the EF2. The EF3 major test includes the aft fuselage section 18 and 19. The EW-test consists of a left wing clamped to a dummy center wing box.

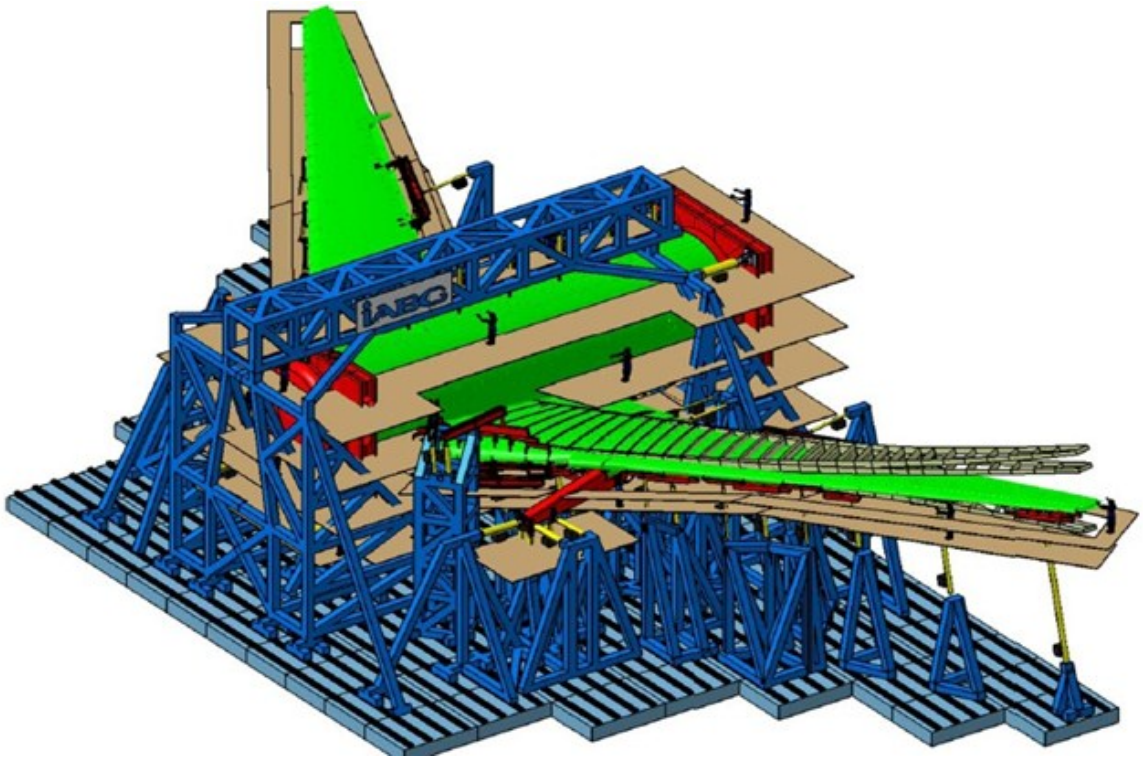

**Figure 2.2 A350XWB EF2 Test**

The external loads will be simulated by about 8 to 88 jacks (dependent on the test), distributed by loading trees to wing ribs or fuselage floor structure.

The loading programme will simulate a minimum of 1 ½ up to 3 design service goals, representing the anticipated typical aircraft usage of a mission mix with short, medium and long range flights. The flight-by-flight sequences will include pressurisation of fuselage, vertical and lateral gusts, vertical and lateral manoeuvres, rotation/lift-off, landing and all events occurring during ground operation like towing/pushback, turning, braking, taxiing, take-off run, landing run.

The test will be split into three major phases 1. fatigue (damage initiation), 2. damage tolerance (damage growth) incl. artificial damages and finally 3. residual strength.

Frequent inspections will be scheduled during the test. These inspections could be general visual, detailed visual and non-destructive inspections.

An artificial damage programme will support fatigue and damage tolerance analysis with damage growth measurements under load redistribution. Monitoring of “accidental damages” and repairs of artificial damages will support development and validation of the structure repair manual (SRM) and establishment of the structure maintenance programme.

Measurement of strains or deflections with strain gauges, ARAMIS system for out of plane displacement measurements, e.g. global buckling pattern and comparison with DFEM, photostress for full field strain measurements and deflection transducers for displacement measurements will be defined.

The test houses EF1 at CEAT in Toulouse, EF2 at IABG in Munich, EF3 at Airbus in Hamburg and EW at IABG in Munich are meanwhile selected.

The test preparation phase is nearly completed, fatigue loading programme in final review, strain gauges installed, inspections defined, i.e. the official test start will come soon (or already started at time of the conference).

## 2.4 A350 NLG Fatigue Test

*T. Grahnert, M. Semsch, G. Lohwaßer (IMA)*

IMA Dresden is performing the Full Scale Fatigue Test for the qualification of the Airbus A350 Nose Landing Gear (NLG). The NLG is developed and manufactured by Liebherr-Aerospace Lindenberg GmbH. Testing started in 2012. Loading and Interface design as well as calculation for strength and stiffness requirements of the loading elements were under responsibility of IMA-Dresden GmbH.

The test shall complete five A/C lives and is still running. The loading of the main load cases for ground loads were realized by 6 hydraulic jacks and 2 passive bars. The loads were introduced via 2 wheel dummies. Furthermore a couple of additional load cases were realized (e.g. for retraction actuator loads). All loads were introduced by a state of the art servo-hydraulic controller system as a flight by flight spectra.

As in previous tests, the performance of comprehensive systems simulations proved to be a valuable tool not only to gain design data for the hydraulic system but also to shorten commissioning and the subsequent optimization of control parameters significantly.

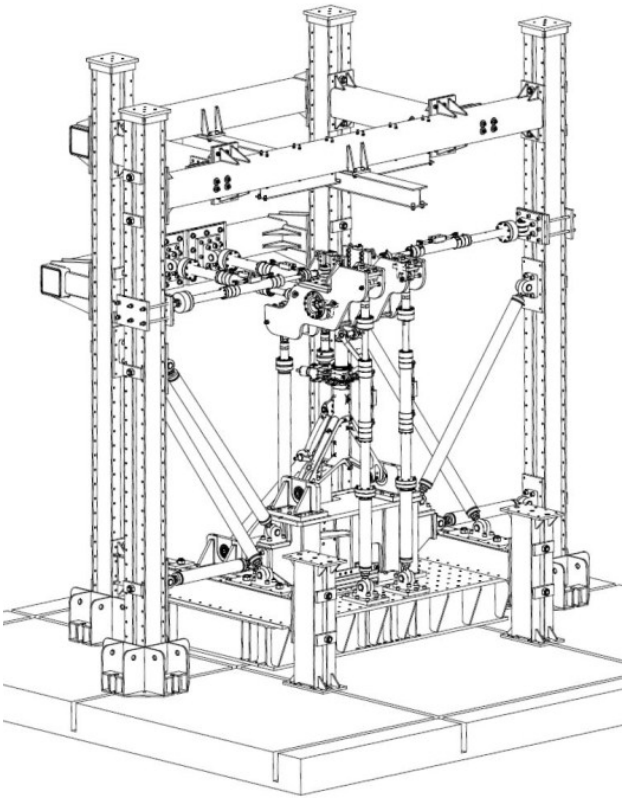

**Figure 2.3 A350 NLG fatigue test set up.**

## 2.5 Fatigue Test of the TORNADO NLG Backup Structure

*G. Hilfer, G. Völlner (IABG)*

The Major Airframe Fatigue Test Set-up of TORNADO which is at IABG since 1980 is still frequently in use for component testing. Currently the Nose Landing Gear Backup Structure is under test. Earlier tests of the structure to fulfill extended qualification requirements brought forth damages which similarly could be found to emerge also on in-service aircraft. After development and installation of a repair solution for the affected parts this repair solution now undergoes testing in order to allow clearance recommendations for the fleet.

Preparation of the scheduled fatigue test was done applying static load cases which were to provide stress data of the modified structure. As part of this static test campaign all 95 load cases making up the fatigue loading program were anticipated and recorded. Furthermore, the stress distribution when activating the retraction jack for lowering/ retracting the NLG was measured.

The fatigue test comprises 13.000 “Test Full-Stop Landings” and 40.000 “Test Retraction and Lowering Cycles” which are arranged in two major blocks. While the full-stop landing load cases are introduced into the aircraft structure by five hydraulic jacks acting on an original nose landing gear installed, the retraction jack loads are introduced using an original retraction jack acting on a landing gear dummy in fully clamped condition. Two further hydraulic jacks and 6 struts are used to take the loads out of the aircraft structure.

Approx. 100 strain gauges are used to perform stress measurement aiming at the validation of numerical predictions and critical locations. Frequent inspections will be performed to check structure integrity and monitor damage growth.

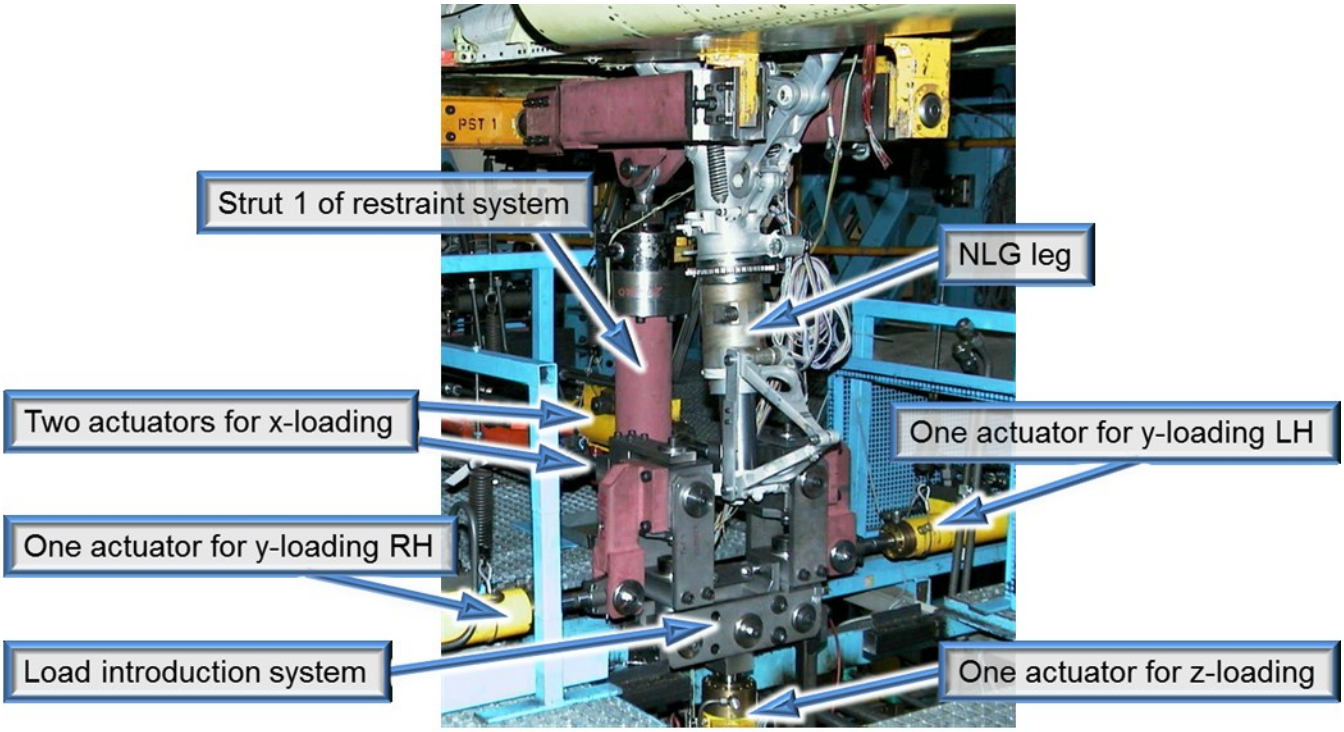


**Figure 2.4 Fatigue Test of the TORNADO NLG backup structure.**

## 2.6 Airbus A400M EF Full Scale Fatigue Tests

*G. Hilfer (IABG)*

In January 2011 IABG entered – as scheduled – the A400M full-scale fatigue test sample in a newly built test hangar at its Dresden test site. The test specimen had been delivered to Dresden before by an Airbus A300ST Beluga.

The test program is required to simulate flights at least one year ahead of the actual operations performed by the aircraft. The test specimen at Dresden, known as MSN5001, has already less than two months later undergone 1,665 cycles, about five times the maximum number of flights expected to be experienced annually by each A400M in service, in order to give a large safety

margin. By mid-2013, 25,000 simulated flights will be performed at IABG's Dresden test site – equating to 2.5 times the A400M´s design-life.

**Figure 2.5 A400M EF Test Set-up**

## 2.7 Real Time Load Simulation

*T. Grahnert, M. Semsch (IMA)*

A fatigue test of a wing component was performed by IMA Dresden from 2010-2012. The specimen was loaded using real-time load measurements from flight tests. This included the introduction of load spectra with frequencies up to 50 Hz.

In total, 10 hydraulic actuators were used to load the specimen at different interface points and bearing supports. The number of forces and actuators and the loading frequencies required some sophisticated actuator and controller set-up. The instrumentation consisted of approximately 120 strain gauge channels and 20 displacement sensors.

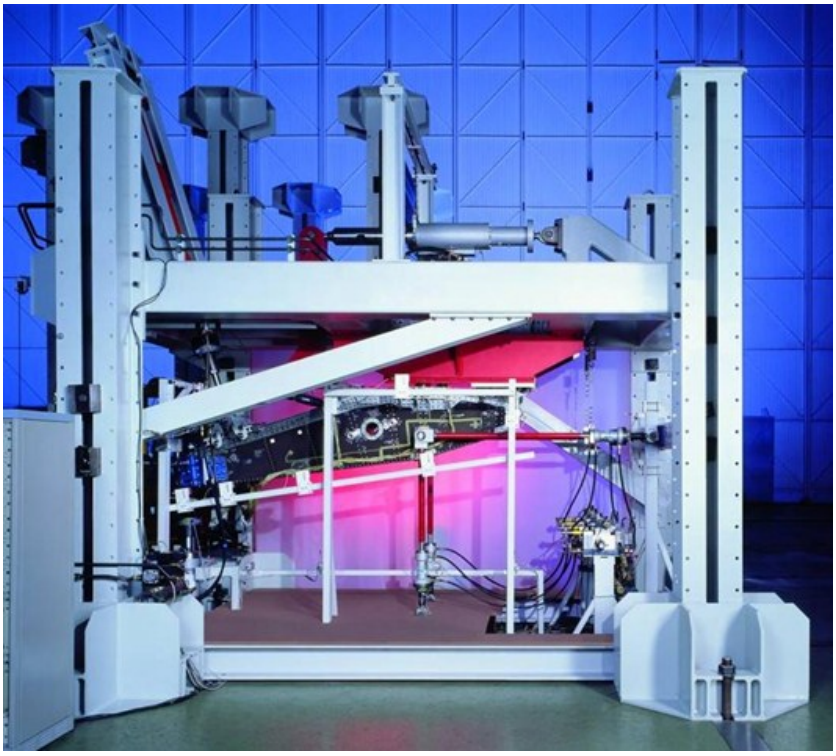

**Figure 2.6 Wing-component test set-up.**

## 2.8 Static and Fatigue Testing of the AW189 Helicopter Main and Nose Landing Gear

*G. Hilfer, N. Abramovici (IABG)*

In 2010, IABG was contracted with the performance of qualification testing for the landing gears of the AgustaWestland Helicopter AW189. Since then, definition, design, build and commissioning of four test rigs progressed and resulted in the start of the testing campaign in late 2012.

Two test rigs were built for Main Landing Gear (MLG) and Nose Landing Gear (NLG) static testing, two other test rigs were built for fatigue testing, respectively. 6 hydraulic actuators are used for loading the single-wheel MLG, 7 actuators are needed for the double-wheeled NLG. All relevant loads like drag loads, braking loads, side loads and retraction/extension loads can be simulated. As well, the shock absorber travel and the relevant roll radius under varying operational conditions can be simulated.

While the static test campaign consisting of limit load (LL) and ultimate load (UL) cases is completed by the time the ICAF symposium 2013 takes place, fatigue testing will still be going on in order to demonstrate 4 lives in total.

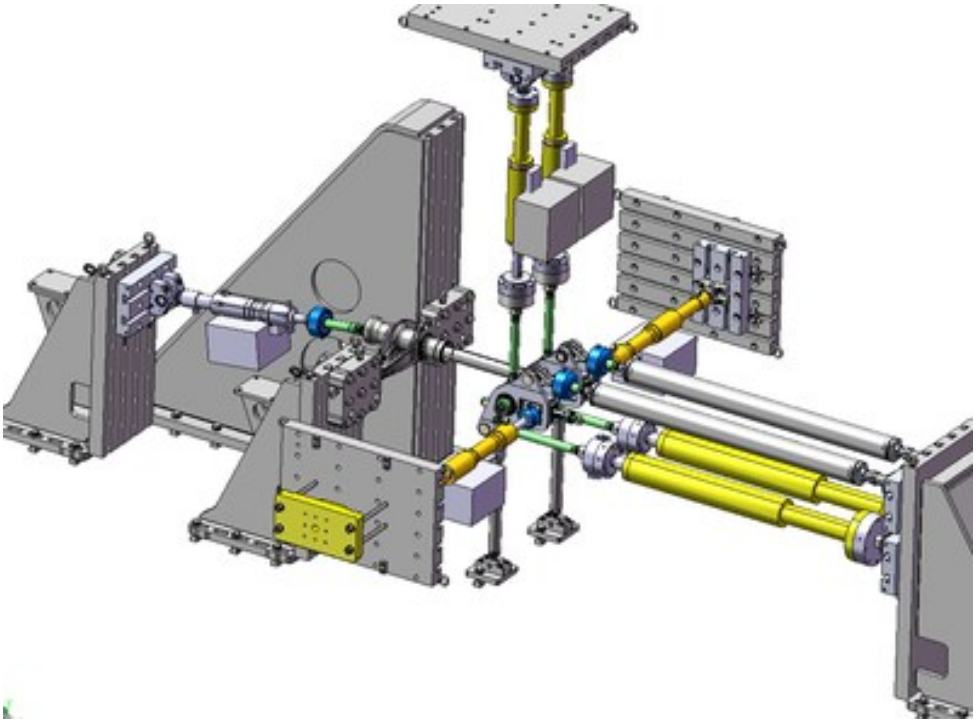

**Figure 2.7 AW189 NLG Test Set-up for static testing (without peripheral test rig).**

# 3 Fatigue and Fracture of Fuselage Panels and Joints

## 3.1 Curved Fuselage Panel Fatigue Testing

*T. Grahnert, M. Semsch (IMA)*

IMA Dresden performed several fatigue tests for metallic curved fuselage panels in 2011 / 2012. The tests were part of research projects in order:

- to evaluate fatigue and damage tolerance behaviour
- to evaluate residual strength
- to compare different materials, designs and construction technologies with regard to these criteria

Fatigue loading was composed from spectrum loading with different flight types. Load components were internal over-pressure and longitudinal tension, representing an upper fuselage panel. In total, five panels were tested.
Furthermore, IMA Dresden put a new test rig into service. Because of the hexapod-like, heavy load introduction structure, the control system of the rig was validated also with respect to its dynamic, fast loading behaviour.

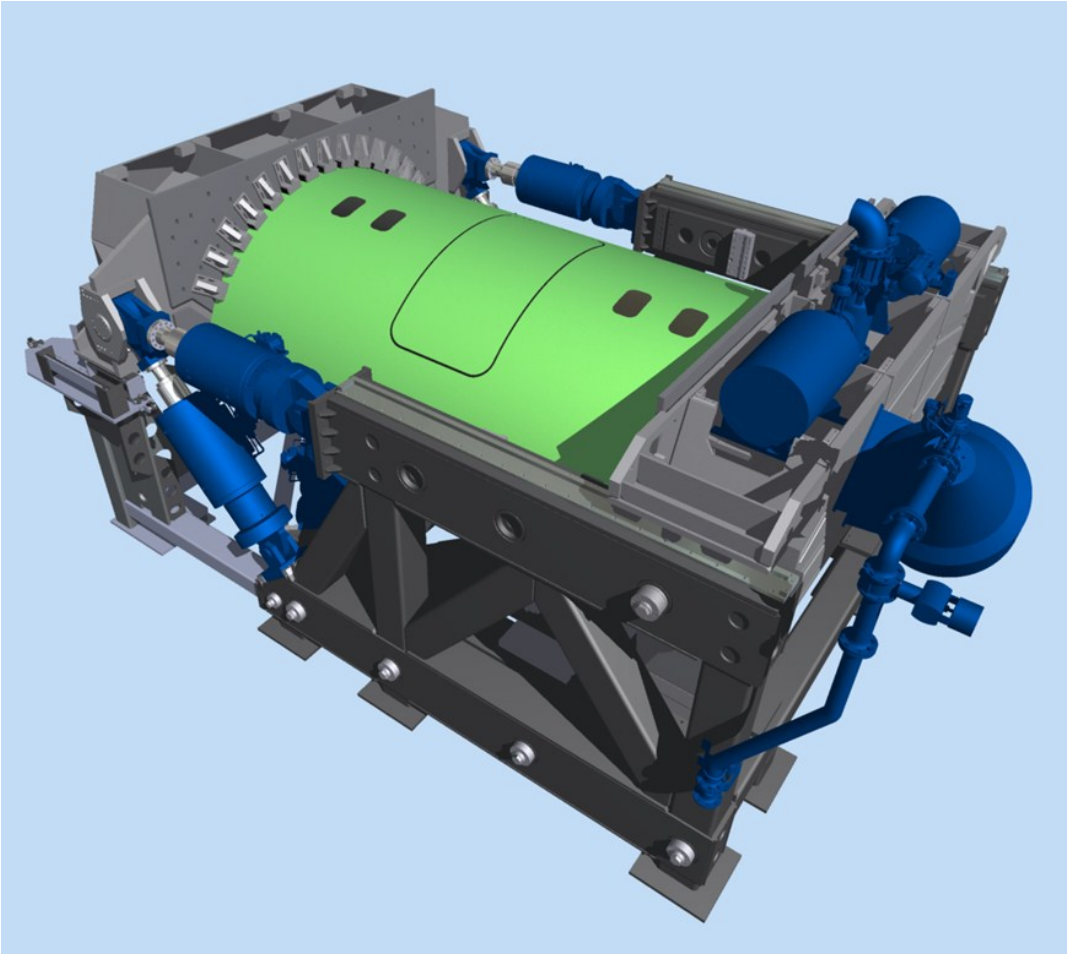

**Figure 3.1 Curved fuselage panel test rig.**

## 3.2 Sonic Fatigue Tests

*T. Grahnert, M. Semsch (IMA)*

Sonic fatigue are carried out to evaluate fatigue to acoustic loading from noise sources on external aircraft structures. Sonic loading is typically in the high cycle fatigue range (up to $10^9$ cycles and more) at a very low level of strain. Coupons representing fuselage skin/stringer panels were excited by narrow-band bending loading of random amplitudes with zero mean load to simulate the stress response due to acoustic loading. To simplify, shakers were used to vibrate the specimens and induce a loading very similar to loads induced by noise. The specimens were excited at their resonance frequency. The reduction of resonance frequency was a sign of fatigue damage. The outcome of the test is fatigue endurance data in form of S/N curves to be used for sonic fatigue certification..

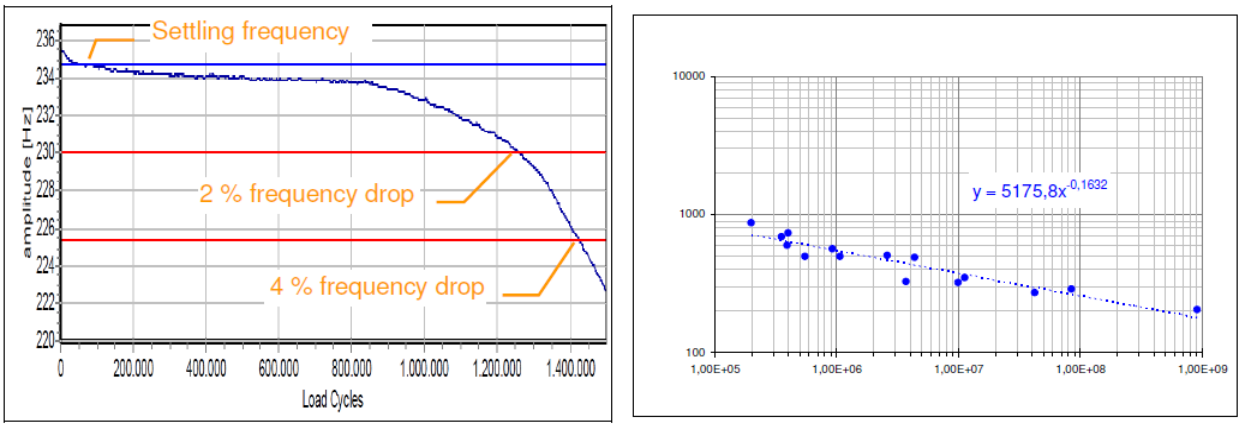


**Figure 3.2 Typical resonance frequency drop in sonic fatigue tests (left) and SN-curve (right).**

## 3.3 Quality assessment of laser beam welded AA2198 integral structures

*N. Kashaev, J. Enz, M. Horstmann, A. Groth, V. Ventzke, S. Riekehr and N. Huber (HZG)*

Design for lower weight generally transforms into higher operating stresses, and damage tolerance becomes a key design driver owing to the loss of structural redundancy. This challenge is addressed by the design philosophy with the development of advanced joining/manufacturing concepts, local engineering, and new computational approaches. Our research targets the validation of the developed laser welding and modification processes for damage tolerance improvement on sub-component level. For this purpose, the LBW process development has being carried out on a large-scale laser welding facility equipped with two 3.5 kW CO2-lasers (Figure 3.3). The facility was installed in cooperation with Airbus Germany and is being used to up-scale the LBW processes for the manufacturing of stiffened panels with stringers on a level that is relevant for a technology transfer. The large-scale facility is comparable to the industrial laser welding facilities of Premium Aerotec, formerly AIRBUS Nordenham. The welding facility of the Helmholtz-Zentrum Geesthacht is capable of up-scaling of the welding process from coupon specimens to complete fuselage panels (8500 mm x 3000 mm). An in-house testing is available for up to five-stringer flat panels of dimensions 900 mm x 1200 mm. High beam quality and low focus diameter of the used CO2-laser beams provide a low energy input per unit length to ensure low distortion of the welded samples.

The accomplished research work addresses the challenges raised by LBW process development for achieving the industrial maturity of this efficient technology for Al-Cu-Li alloys of the 3rd generation, AA2196 and AA2198. As the result of the process development, fillet joints without lack of penetration have been produced from Al-Li alloys [1,2].

In comparison with other Al-alloys, the present laser beam welded joints exhibited good mechanical properties in spite of some weak spots such as porosity. In this respect, the AA2198–AA2198 alloy combination in particular showed good weldability and exhibited the best performance in the pull-out test, although this combination had a slightly inferior tensile strength in the hoop-stress test [1]. Fatigue crack growth behaviour of the welded four-stringer panels was found to be comparable to that of the base material (Figure 3.4). Insofar the weld had reasonably good mechanical properties. This indicates that high quality laser beam welds of AA2198 can be produced using the developed laser welding process [3].

**References**

[1] Enz, J., Riekehr, S., Ventzke, V., Kashaev, N., Huber, N. (2012), Welding and Cutting, vol. 64, n. 8, pp. 482-485.

[2] Enz, J., Riekehr. S., Ventzke, V., Kashaev, N. (2012), Physics Procedia, vol. 39, pp. 51-58.

[3] Kashaev, N., Enz, J., Horstmann, M., Groth, A., Ventzke, V., Riekehr, S. and Huber, N. (2013), In: Proceedings of the 27th ICAF Symposium, Jerusalem, submitted.


a) b)

**Figure 3.3 (a) Large scale laser beam welding facility of the Helmholtz-Zentrum Geesthacht and (b) welded demonstrator panel from aluminium alloy AA2198.**

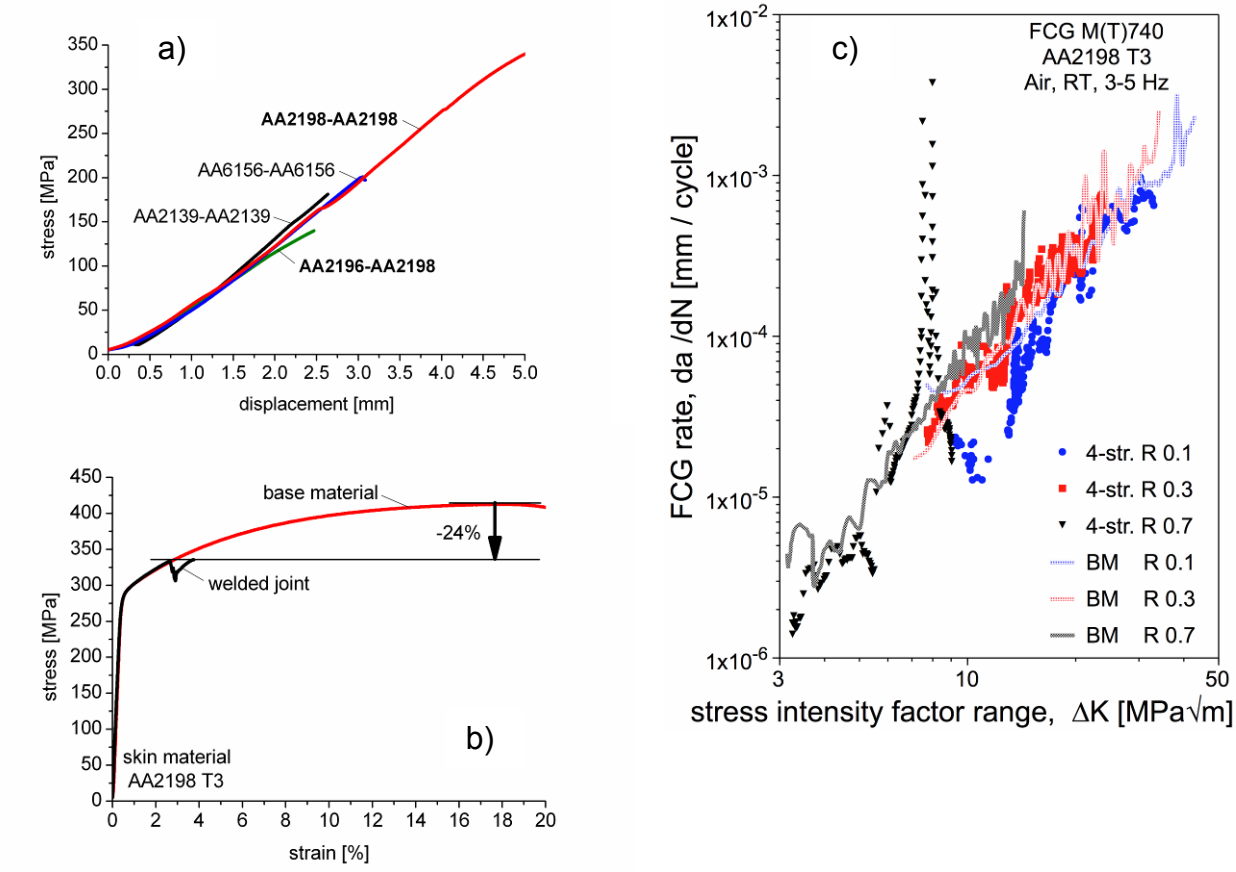


**Figure 3.4 (a) Results of the pull-out test, (b) the hoop-stress test and (c) the fatigue crack growth behaviour of the laser beam welded four-stringer panels, load ration effect.**

## 3.4 High-frequency cyclic testing of welded aluminium alloy joints in the region of high cycle fatigue (HCF) and very high cycle fatigue (VHCF)

*M. Cremer (LMW), M. Zimmermann (TUD), H.-J. Christ (LMW)*

High-frequency fatigue tests on welded samples with trimmed surfaces (without weld reinforcement) were carried out by means of an ultrasonic fatigue testing system (UFTS) with working frequencies of about 20 kHz. Because of the wave-like distribution of the load amplitude along the longitudinal axis of the UFTS specimens, with a maximum in the minimum cross-section (at about the half length) of the sample, a selective testing of the different weld zones, the weld seam (WS), the heat-affected zone (HAZ) and the base material (BM) is possible. This permits a separate evaluation of the influence of each zone on the HCF and VHCF behaviour. Figure 3.5 depicts the fatigue results and demonstrates that none of the weld zones exhibits a fatigue threshold beyond the classical limit ($N \geq 2 \cdot 10^6$) but a rather continuous decrease in fatigue strength. The precipitation-hardened EN AW-6082 BM with a Vickers hardness of 110 HV shows the highest fatigue strength, followed by the HAZ of the same material. Fatigue behaviour of both the BM and the HAZ is strongly influenced by different microstructural effects. Samples out of the HAZ of the work-hardened EN AW-5083 did not fail in the highest stressed cross section but in the area of the weld seam (about 8 mm below the surface) because of various weld defects. Results of the WS out of the filler material Al S 5183 show a drastic decrease of

cyclic strength compared to all other zones and represent the weakest link. Results of the BM and the HAZ out of EN AW-6082 are within the distribution range of the master S-N curve as suggested by Morgenstern et al. [1]. A comparison with the WS with run-outs at each stress levels and a large scattering raises the question whether theories based on local approaches are the right fatigue assessment for the VHCF range compared to fracture mechanic approaches.

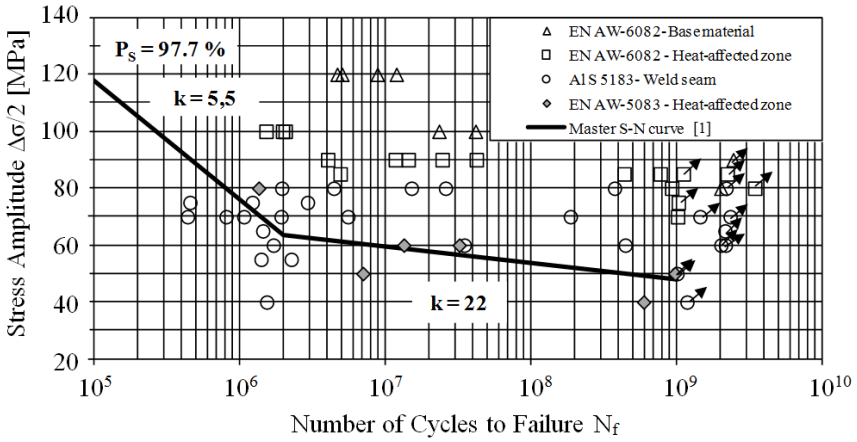


**Figure 3.5 S-N data of welded samples with trimmed surfaces representing the different welding zones weld seam (WS), heat-affected zones (HAZ) and base material (BM) tested at a stress ratio R=-1 in comparison with the master S-N curve from [1] with a probability of survival $P_s$ = 97.7 % (arrows denote run-outs).**

Fracture surface and in-situ thermography analysis indicated a tendency towards earlier crack initiation at the areas of incomplete fusions and further propagation of the crack is supported by pores in the interior of the weld seam. This demonstrates the influence of weld inhomogeneities, their geometry, size and position on the fatigue behaviour of these aluminium weld seams in the HCF and in the VHCF range. In addition, “artificially” notched and heat-treated samples with the same notch factor compared to the weld reinforcement, representing the macroscopic notch effect of the welded joint, were investigated. The results for the HCF and VHCF behaviour of artificially notched samples can be seen in Figure 3.6. It could be proven that the fatigue behaviour beyond the classical fatigue limit does not solely depend on the macroscopic notch. In fact, the cyclic strength depends on microstructural effects as can be seen by the results for the artificially notched samples (all with similar notch factor) in various heat-treatment conditions (max. precipitated with 110 HV, over-aged with 85 HV and 75 HV).

Comparison of the results of smooth samples (continuous line in Figure 3.6) and notched samples (dashed line in Figure 3.6) out of EN AW-6082 with 110 HV indicates a reduction of cyclic strength of about 35%. However, future investigations on welded samples with reinforcement and varying weld quality will have to prove, whether the pronounced influence of the welding defects will remain the life limiting feature. Future fatigue assessment approaches for welded joints will be oriented on probabilistic fatigue life evaluations based on defect size and position combined with fracture mechanics analysis as well as studies regarding microstructural effects.

## Reference

[1] C. Morgenstern (2006): Kerbgrundkonzepte für die schwingfeste Auslegung von Aluminium-Schweißverbindungen am Beispiel der naturharten Legierung AlMg 4, 5Mn (AW-5083) und der warmausgehärteten Legierung AlMgSi 1 T6 (AW-6082 T6), Dissertation, TU Darmstadt.

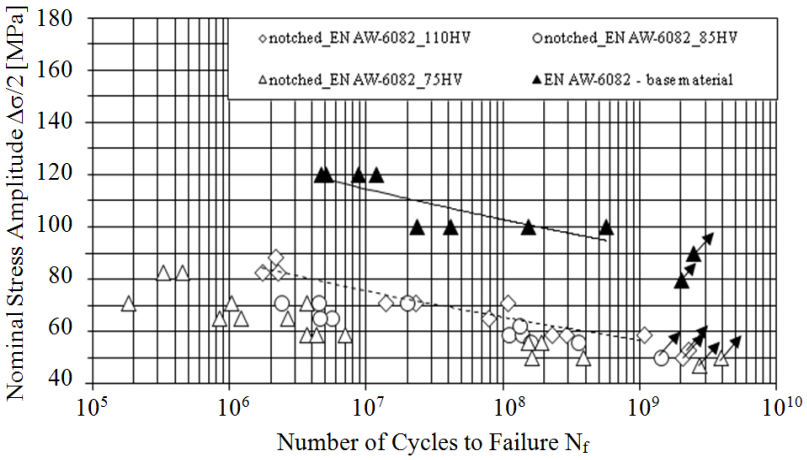


**Figure 3.6 Fatigue results for artificially notched specimens (R = -1) in different heat treatment conditions in comparison with smooth samples from the base material in the peak-aged condition (arrows denote run-outs).**

## 3.5 Fatigue and Damage Tolerance of GLARE structures subjected to impact loading

*R Starikov (Airbus)*

Various impacts by foreign objects to aircraft fuselage structures are to be expected during in-service operations. The introduction of GLARE (GLAss REinforced) laminates as skin material for selected fuselage shells of Airbus A380 required the assessment of the impact and post-impact behaviour of GLARE under aircraft representative loads in order to define impact allowable damage limits, ADL, (i.e. damage for which a structural repair is not necessary, and/or justified with an inspection interval the structure can be operated).

Coupon GLARE laminates with different configurations were impacted with various energies in order to introduce different extent of impact damage. Dents with different shapes, as a result of plastic deformation of aluminium sheets; and being a stress concentration, would affect the fatigue behaviour of impacted GLARE differently. On the other hand, delaminations are the main concern when the impact behaviour of laminated materials is addressed. Consequently, all impacted coupons were tested in fatigue (see Figure 3.7).

The laminate configuration and material properties of the forming metallic and composite constituents have significant influence on the impact and fatigue behaviour of GLARE. Similar to composites, the properties of GLARE follow the "rule of mixture", so called "Metal Volume Fraction". This means that there is relationship which makes it possible to predict the impact behaviour of GLARE laminates with different material constituents and configuration [1]. Fatigue cracks initiated and propagated in the outer metal sheet at the dent boundary in the impacted side of the laminates. Thanks to the crack bridging effect, the growth of fatigue cracks was very stable. The fatigue behaviour of the coupons was depended on the stress level in the cracked sheet and the geometry of particular dent: the more shallow dents were, the longer their fatigue life was (see Figure 3.7) [2]. Since the coupon investigation did not cover all GLARE configurations used on the A380, using the Metal Faction Approach and available experimental data on the impact and fatigue behaviour of selected GLARE laminates as reference, it was possible to predict the impact and F&DT response of dented GLARE with different configurations.

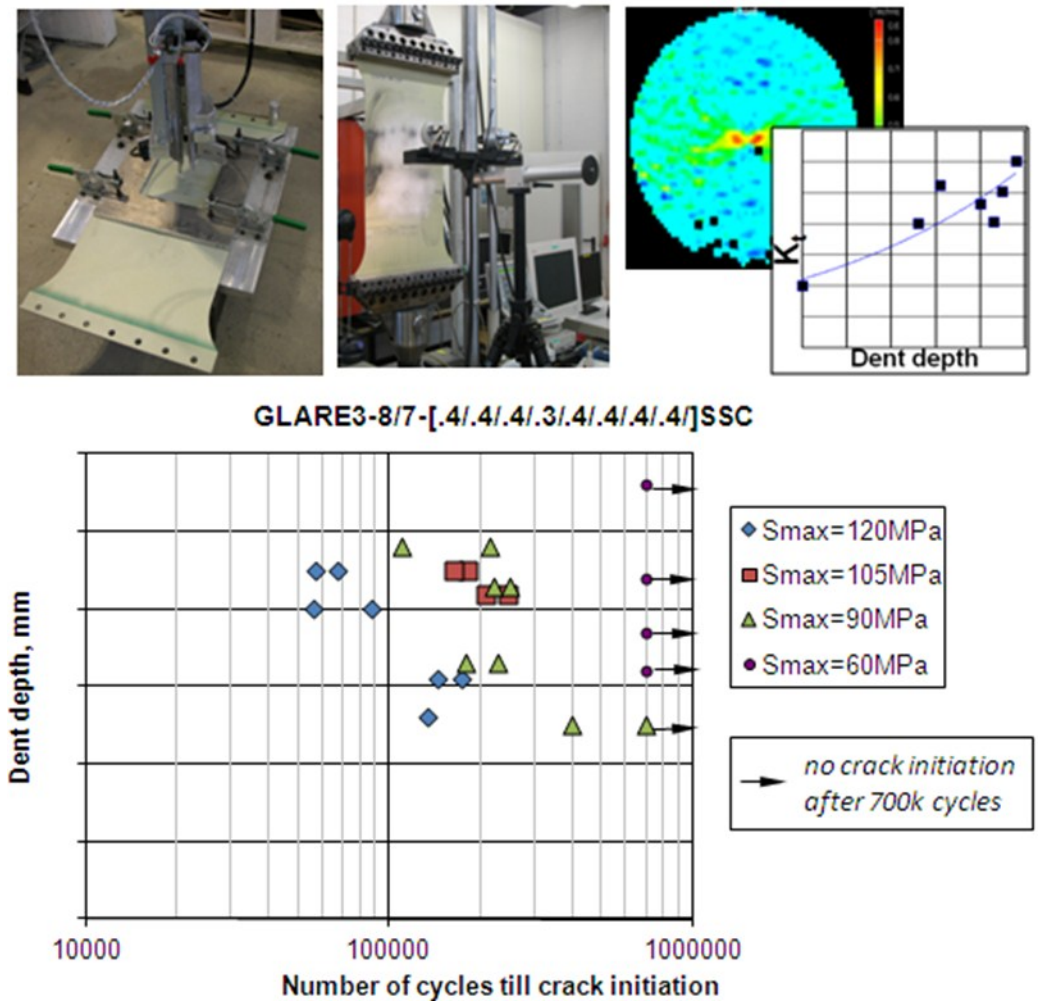


**Figure 3.7 Fatigue assessment of impacted GLARE.**

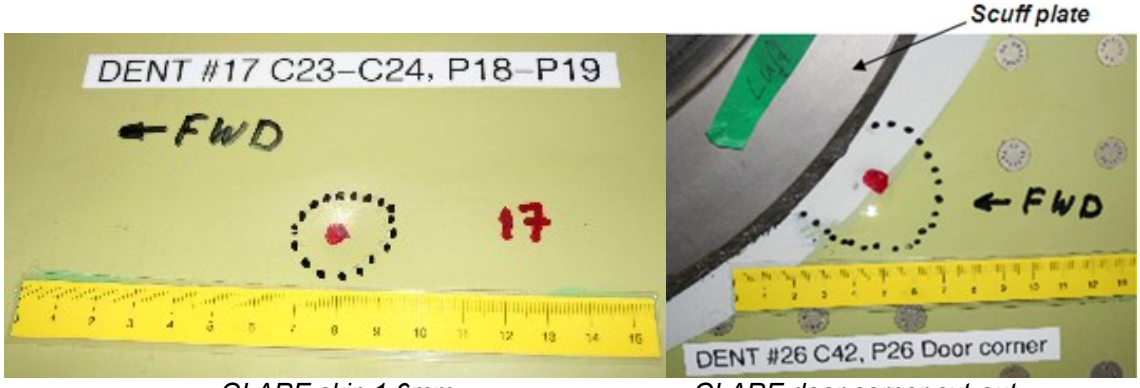


*GLARE skin 1.6mm, 4.5mm dent due to 90J impact*

*GLARE door corner cut-out 2.2mm dent due to 2x90J impact*

**Figure 3.8 Selected GLARE dents introduced on A380 FSFT.**

Although, the definition of GLARE dent ADLs is mainly based on the outcome of the coupon investigation, in total 45 impacts were performed on selected GLARE panels of the A380 FSFT (Full Scale Fatigue Test). The impact locations included skin pockets, skin over bonded and riveted stringers, fuselage joints, door surroundings, and window frames mounted into GLARE skin (see Figure 3.8).

The results of full-scale testing were used not only to support the ADL definition, but to justify the effect of different boundaries between the coupons and full-scale structure. For instance, comparison of both sets of the results indicated that the A380 FSFT GLARE skin impacts required higher energy in order to introduce dents with similar depths as the ones in the flat coupons. The A380 FSFT GLARE dents introduced in skin far-field areas were loaded for 42300 flight cycles, which is ca 2.2 A380 Design Service Goal with an enhancement factor of 1.1 on all loads including internal pressure. Neither fatigue cracking nor growth of impact delaminations were reported by NDI during and at the end of the A380 FSFT campaign.

### Conclusions

The definition of GLARE dent ADLs is based on the outcome of coupon testing and supported by the full-scale test results. The presence of indents makes it easy to visually allocate the location of accidental damage, check the presence of impact cracks, and perform dent depth measurements. The introduction of GLARE can in fact allow a new approach to the maintenance procedures existing for fuselage aluminium skins. Thanks to the direct dependency of the F&DT performance of impacted GLARE on the properties of laminate constituents, the dent shape, and fatigue stress levels, the mechanical response of particular dented skin pocket can be predicted in order to define moments for maintenance actions, if any, to take place. Such a mapping of GLARE dent ADLs would make the aircraft operability more efficient, flexible, and cost saving for A380 operators.

### References

[1] R Starikov “Assessment of impact response of fiber metal laminates“, International Journal of Impact Engineering, accepted for publication, 2013.

[2] R Starikov “Fatigue resistance of composite fiber metal laminates subjected to impact loading”, ECCM-13, Stockholm, Sweden, 2008.

# 4 Fatigue Life Assessment and Prediction

## 4.1 Influence of overloads on the crack formation and propagation in EN AW 7475-T761

*J. Bär and G. Wilhelm (UniBwM)*

The knowledge of the fatigue behavior under spectrum loading is essential for realistic life time predictions. A first step is the understanding of the influence of single overloads on the fatigue behavior. Fatigue tests have been performed on CCT-Specimens of an AW7475-T761 clad sheet material with maximum stresses of $\sigma_{BL}$=160, 180, 200, 240 and 280 MPa, respectively and a load ratio of R=0. Overloads with a maximum stress of 150% of the base load were introduced in equally spaced cycle numbers of $N_{OL}$=100, 1000 and 10000 cycles, respectively. For crack detection and crack length measurement a DC potential drop method was used. The crack length was calculated from the measured potential drop.

Figure 4.1 shows the crack length as a function of the cycle number for a fatigue experiment with a base load $\sigma_{BL}$ =280 MPa and an overload spacing of $N_{OL}$=1000. At the beginning, a fast increase of the crack length up to 0.2 mm is visible. This slight increase is followed by a plateau region which dominates the cyclic lifetime. In the plateau-region a slight increase of the crack length of about 0.1 mm can be observed. The crack length in the plateau-region exhibits a great scatter of about ±0.08 mm around the mean value. It is clearly visible that the plateau-region covers more than 80 % of the cyclic lifetime. The end of the plateau-region reflects in the start of the propagation of a macroscopic fatigue crack, indicated by a significant increase of the potential.

To get more information about the early stages of crack propagation during fatigue, crack surfaces have been investigated by using SEM. On the crack-surface traces caused by the overloads are visible. With rising crack length the overload induced traces get more pronounced. Starting from the final fracture the cycle-number of the traces can be determined. In Figure 4.2 the region near an incipient crack is shown. The trace induced by the overload Nr. 10 is labeled by arrows. After 10000 cycles the crack length at the surface was about 85 µm and in the depth more than 50 µm. On the right hand side the 7th overload can be discovered, on the left hand side even the second one (N=2000), too. This result demonstrates that an incipient crack is generated in less than 2000 cycles, i.e. 5% of the cyclic lifetime. Consequently, the plateau-region has to be correlated with the propagation of small fatigue cracks.

The investigations have shown that the propagation of long fatigue cracks covers less than 20 % of the total lifetime, the crack initiation only about 5%. Therefore most of the cyclic lifetime is concerned with the propagation of short cracks. Unfortunately the DC-potential drop method is insensitive to investigate the propagation of short cracks. Consequently, the small increases in the crack length in the plateau-region don't lead to a considerable increase of the potential drop. Solely at higher base loadings a noticeable increase of the potential in the plateau region can be found. However, the investigation of the crack surfaces of specimen loaded with overloads has shown that in the plateau region the propagation of short fatigue cracks can be observed. In case of experiments without overloads it can be assumed that in the plateau-region the propagation of small fatigue cracks takes place, too. With this consideration crack formation can be neglected and nearly the complete cyclic lifetime can be contributed to crack propagation. Therefore, the influence of periodic overloads nearly covers the complete lifetime which is in

accordance with the experimental results where the region of macroscopic crack propagation as well as the plateau region is influenced by the overloads in the same matter.

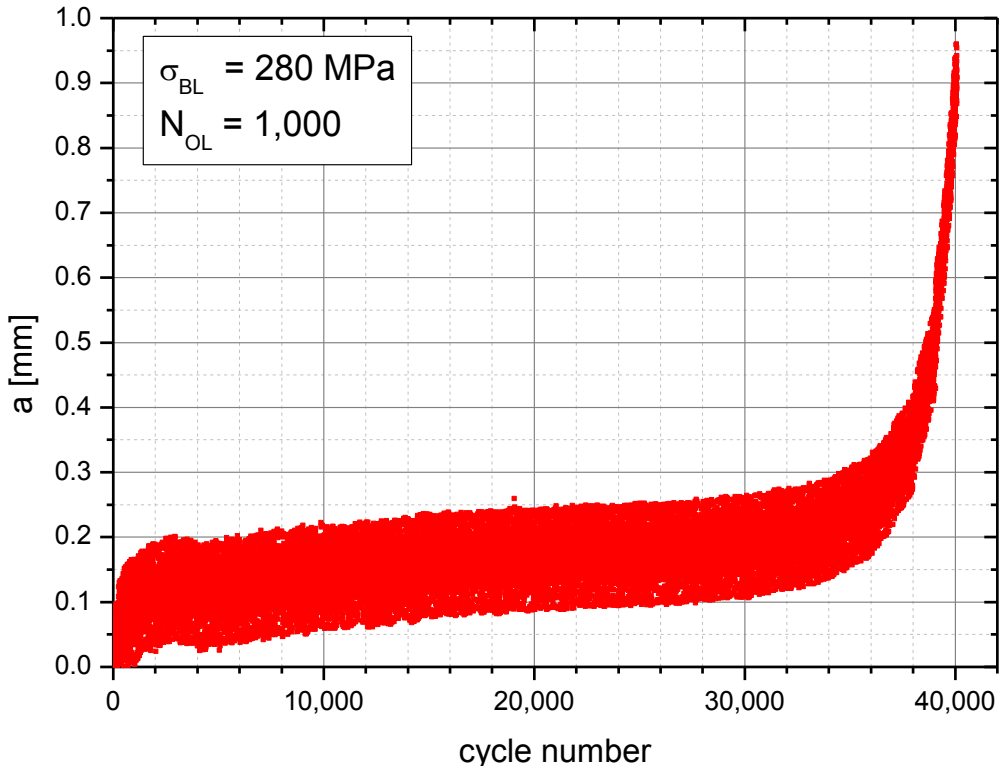


**Figure 4.1 crack length vs. cycle number for fatigue test with $\sigma_{BL}$ = 280 MPa and $N_{OL}$ = 1000.**

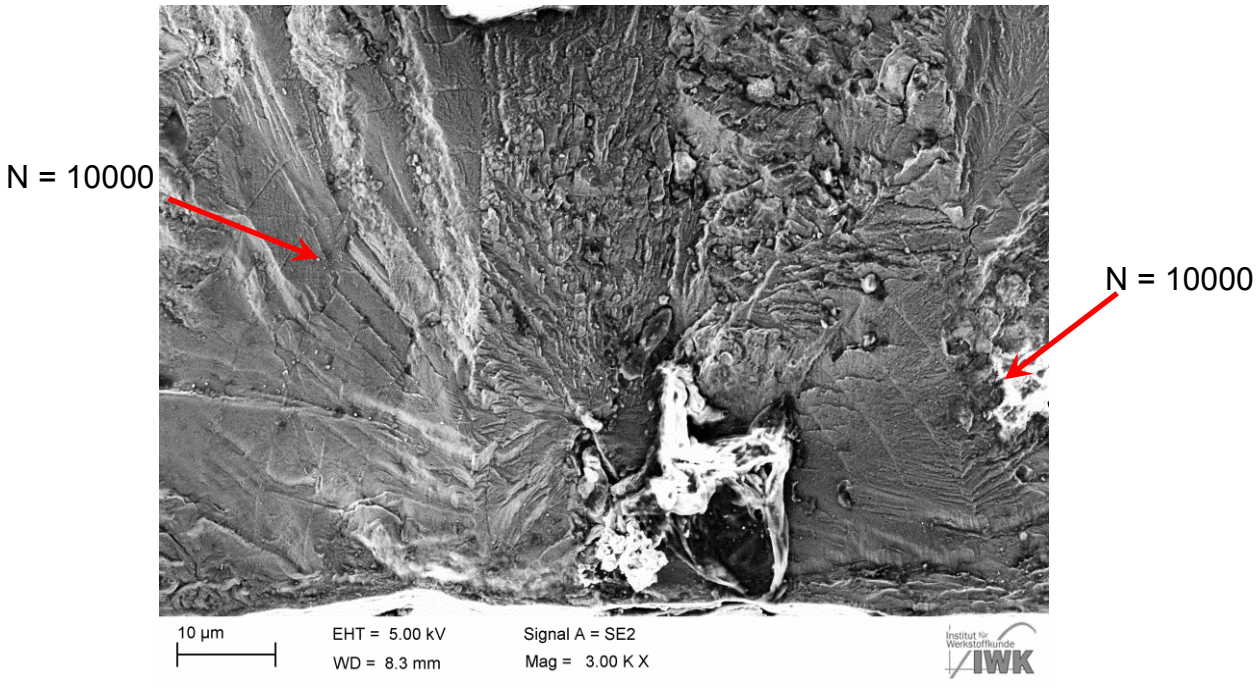


**Figure 4.2 Crack surface of specimen-loaded with $\sigma_{BL}$ = 280 MPa and $N_{OL}$ = 1000.**

For fatigue lifetime predictions taking periodic overloads into account, solely the crack propagation has to be taken into consideration. The effect of single overloads seems to be the same in case of long and short fatigue cracks. This allows a common description of the influence of single overloads on the propagation behavior of long and short fatigue cracks and therefore the lifetime of cyclic loaded specimen.

## 4.2 Laser heating as an approach to modify residual stress states in thin-walled aluminium structures

*A. Groth, D. Schnubel, N. Kashaev and N. Huber (HZG)*

A promising way to improve the damage tolerance of lightweight structures is the modification of their residual stress states [1]. Well known possible ways to influence residual stresses are mechanical and thermal processes that can be applied during the production of the structural components. Also the post-treatment of welded components by annealing is a common method for improving local mechanical properties and for removing unfavourable residual stresses. However, a heat treatment of welded components should be avoided due to high costs and, in case of precipitation strengthened alloys, the change of the mechanical properties of the base materials.

As one possible solution, local laser heating was applied to AA2198 aluminium alloys as a post-treatment for introducing a residual stress field which is optimized for the retardation of fatigue crack growth [2-5]. For the process development, C(T)100 specimens were manufactured out of rolled AA2198 material of 5 mm thickness. The local laser heating was applied by a defocused laser with a spot size of approximately 5 mm along a line perpendicular to the crack direction at distances between 5 mm and 65 mm from the initial crack tip. For the understanding the development of the residual stresses during the laser heating and for later optimization of the positioning of the laser heating line, the heating process as well as the crack growth were simulated by FE methods. The simulation of the laser heating process was carried out using SYSWELD by combining a heat flux simulation and a subsequent mechanical simulation to determine the resulting residual stresses. Finally, the capability of the stress field to retard or even suppress crack growth has been investigated in a fracture mechanics simulation combining ABAQUS with the MVCCT method and the Walker equation for the prediction of the fatigue crack growth rate, as shown in Figure 4.3.

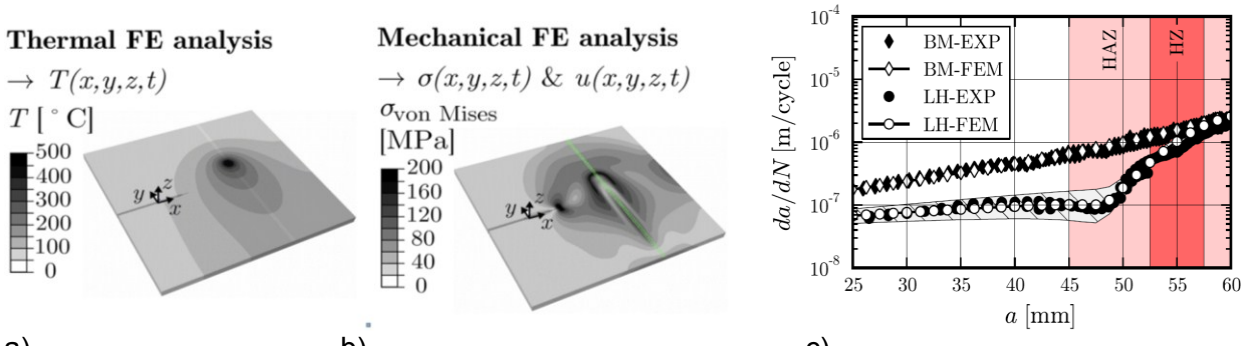


**Figure 4.3: (a) Results of the thermal and (b) mechanical simulation; (c) numerical predictions and the experimental results for the crack growth rates in unmodified (BM) and laser heated (LH) material (c) – HZ: Heating Zone of the laser heating process; HAZ: Heat Affected Zone [4].**

It was shown that the compression residual stresses, which distribute into a region far from the laser heating line (> 30 mm to both sides), have a remarkable retardation effect on the fatigue crack growth. As a result, the lifetime of the C(T)100 specimen can be extended by more than 100% [4,5]. Based on these very promising results, the on-going work aims at the implementation of the described laser heating procedure for the residual stress design of larger structures produced from AA2024 sheet material of 2 mm thickness without and with stringers (Figure 4.4). To this end, an efficient up-scaling of the process simulation will be the key for the optimization of the positioning of the laser heating lines in these structures. To improve the computational efficiency, the process simulation was transferred from the hybrid SYSWELD/ABAQUS approach to ABAQUS. Furthermore, the 3D solid model for the process simulation has been replaced by a 3D shell model without loss of information and accuracy. The verification of this approach with the existing results for AA2198 has shown that a re-calibration of the heat source amplitude $Q_0$ is required to achieve the same result. This can be explained by the different position of the integration points in the elements in SYSWELD and ABAQUS. The next steps aim at the fracture mechanics simulation of the larger structures and the systematic evaluation of the retardation effect in such structures.

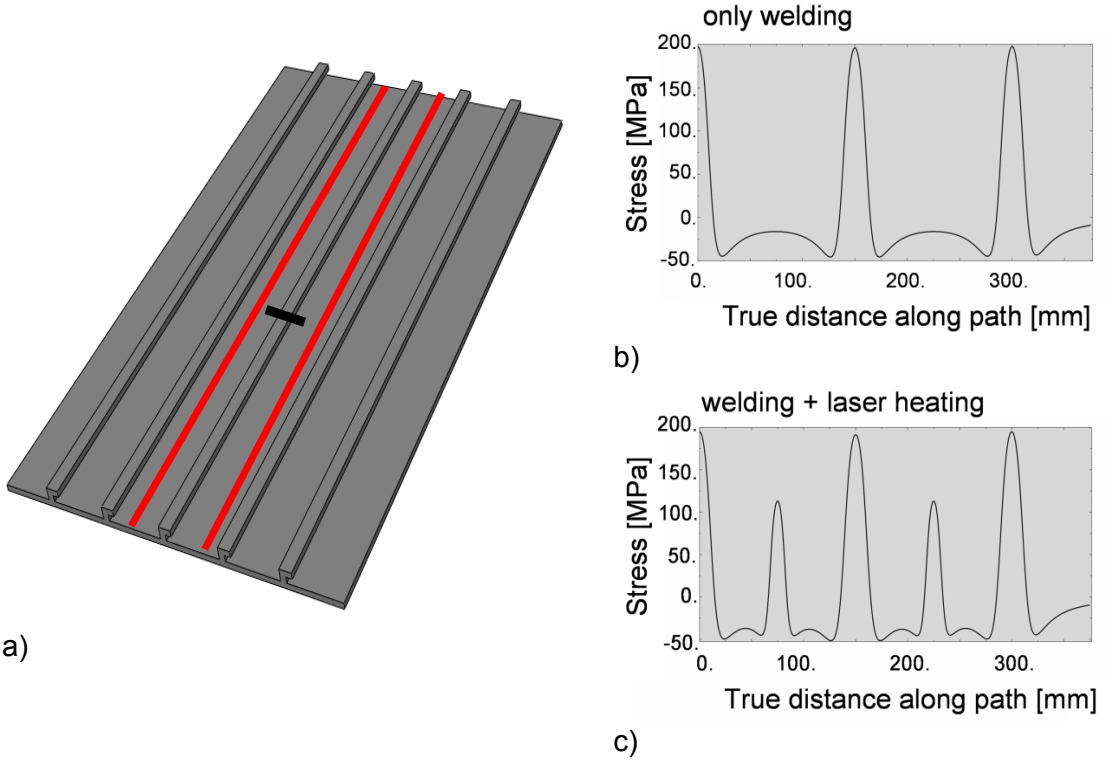


**Figure 4.4 (a) five-stringer panel and results of the residual stress modelling (b) for the panel with welded stringers and (c) for the panel with welded stringers and two laser heating lines between stringers.**

## References

[1] Masubuchi, K. (1980), Analysis of welded structures: Residual stresses, distortion, and their consequences, Pergamon Press.

[2] Schnubel, D., N. Huber, N. (2012), Engrg. Fract. Mech., Vol. 84, pp. 15-24.

[3] Schnubel, D., et al. (2012), Materials Science and Engineering A, Vol. 546, pp. 8-14.

[4] Schnubel, D., Huber, N. (2012), Computational Materials Science, Vol. 65, pp. 461-469.

[5] Schnubel, D., Horstmann, M. and Huber, N. (2013), In: Proceedings of the 27th ICAF Symposium, Jerusalem, submitted.

### 4.3 Universal Mathematics and Physics: Dimensions and Units Relativity

*Lev G. Gelimson (AICFS)*

Physical and mathematical modelling and measurement are based on the unity and relativity of abstractness and concreteness, as well as of quality and quantity. Excessive abstractness can lead to losing physical sense, e.g. of probability densities, via ignoring or mixing distinct measurement units, e.g. in approximation and empirical formulae in physics and by different dimensions units in mathematics.

Universal mathematics and physics [1-5] introduce the canonic one-dimensional unit $U = Q]0, 1] = \Omega^n$ (uniquantity Q as a universal point measure; Ω the continuum cardinality ℂ) and its powers $U^r$. $U^0 = 1$ is the absolute unit interpretable via anyone point. Pointwise probability distribution function g(x) explicitly expresses the strictly positive uninumber [1-4] probability that any random variable X takes namely the value x from point set S(X). Additionally discover the both mathematical and physical sense of classical probability density, or differential probability function, f(x). It is natural and corresponds to the axioms system of classical probability theory that namely the integral probability function F(x) varying between 0 for impossible events and 1 for certain events is always one-dimensional pure-number. Hence its unit UF(x) = U . Denote Ux the unit and Vx the usual value of x , as well as Ug(x) the unit and Vg(x) = f(x) the usual value of g(x). Then $\int_{x\in X} Vg(x)\, d(Vx) = \int_{x\in X} Vg(x)\, Ux^{-1}\, d(Vx\, Ux) = 1 = U^0$ as usual by ignoring units. For the desired equality $\int_{x\in X} g(x)\, dx = 1 = U^0$, it is necessary and sufficient that $Ug(x) = Ux^{-1} = 1/Ux$ and $g(x) = Vg(x)\, Ug(x) = f(x)\, Ux^{-1}$. Hence f(x) = g(x) Ux and has the sense of the product of the pointwise probability distribution function g(x) and of the variable unit Ux . If X and hence x are, e.g., n-dimensional ($n \geq 1$) with $x = (x_1 , x_1 , \dots , x_n)$, then $Ux = \Pi_{i=1}^n Ux_i$ , $Ug(x) = 1/\Pi_{i=1}^n Ux_i$ , and $g(x) = f(x) / \Pi_{i=1}^n Ux_i$ . If $Ux_1 = Ux_2 = \dots = Ux_n$ , denote this common unit as Ux' and obtain $Ux = Ux'^n$, $Ug(x) = 1/Ux'^n$, and $g(x) = f(x)/Ux'^n$. If all the n coordinates $x_i$ are one-dimensional pure-number whose units $Ux'_i$ are simply U , then $Ux = U^n$, $Ug(x) = 1/U^n$, and $g(x) = f(x)/U^n = f(x)/\Omega^n$ in the universal point measure. If n = 1, then Ux = U, Ug(x) = 1/U , and g(x) = f(x)/U = f(x)/Ω. New simple and very suitable bounded continual distributions with explicit both integral and differential distribution functions provide efficiently fitting known and unknown distributions and estimating given data. Normal integral distribution function approximation with mean m and variance $\sigma^2$

$$\Phi_{m\,,\,\sigma\,,\,k}(x) = 0.5[1+\mathrm{sign}(x-m)] - 0.5\ \mathrm{sign}(x-m)\ e^{0.5}\exp\{-[x - m + \mathrm{sign}(x-m)\ k^{0.5}\ \sigma]^2/k/2/\sigma^2\}$$

by $k = \pi/2$ provides the exact value $\varphi_{m\,,\,\sigma\,,\,\pi/2}(x) = 1/[(2\pi)^{1/2}\sigma]$ and the relative errors at most 0.7 % by $x \geq 0$ and by k=1.5 the relative errors less than 0.4 % (Figure 4.5Figure 4.6).

Analytically fitting any normal integral distribution function via an appropriate proportionally transformed normal differential distribution function also provides the coincidence of their inflection points. That is much more suitable than exclusively tabular data on the only standard normal integral distribution function with m = 0 and σ = 1, which requires recalculation in computing. This is especially important because namely normal distributions are the most typical in nature, science, and engineering.

Universal mathematics and physics create fundamentally new opportunities to obtain reliable measurement data even by great data scatter, e.g. in aeronautical fatigue, and to discover new phenomena and laws of nature and science.

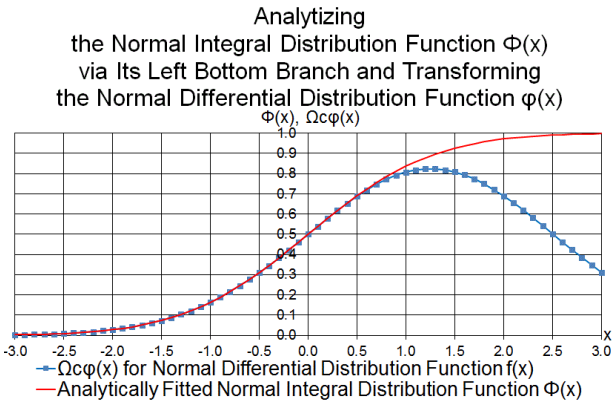


**Figure 4.5 Analysing normal Φ(x) via φ(x)**

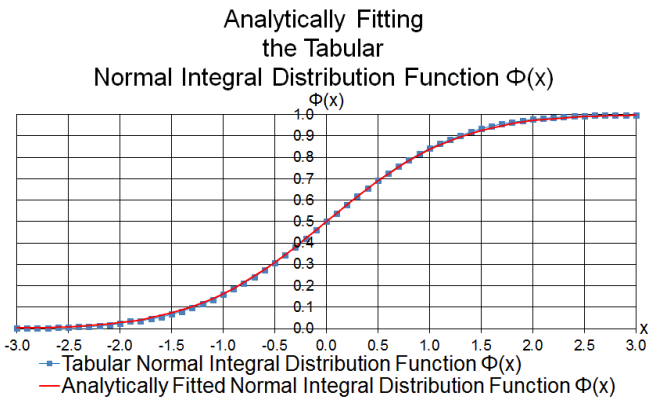


**Figure 4.6 Quality of analytically fitting tabular normal distribution function Φ(x)**

## References

[1] Lev Gelimson. Quantianalysis: Uninumbers, Quantioperations, Quantisets, and Multiquantities (now Uniquantities). Abhandlungen der WIGB (Wissenschaftlichen Gesellschaft zu Berlin), 3 (2003), Berlin, 15-21

[2] Lev Gelimson. General Problem Theory. Abhandlungen der WIGB (Wissenschaftlichen Gesellschaft zu Berlin), 3 (2003), Berlin, 26-32

[3] Lev Gelimson. Elastic Mathematics. General Strength Theory. The "Collegium" All World Academy of Sciences Publishers, Munich, 2004

[4] Lev Gelimson. Providing Helicopter Fatigue Strength: Flight Conditions. In: Structural Integrity of Advanced Aircraft and Life Extension for Current Fleets – Lessons Learned in 50 Years After the Comet Accidents, Proceedings of the 23rd ICAF Symposium, Claudio Dalle Donne (Ed.), 2005, Hamburg, Vol. II, 405-416

[5] Lev Gelimson. Providing Helicopter Fatigue Strength: Unit Loads. In: Structural Integrity of Advanced Aircraft and Life Extension for Current Fleets – Lessons Learned in 50 Years After the Comet Accidents, Mechanical and Physical Journal of the 23rd ICAF Symposium, Claudio Dalle Donne (Ed.), 2005, Hamburg, Vol. II, 589-600.

## 4.4 Universal Metrology (Measure and Measurement Sciences)

*Lev G. Gelimson (AICFS)*

Measurement along with probabilistic and statistical analysis is based on measures.
In classical and modern mathematics [1] and physics [2], there is no perfectly sensitive universal measure with conservation laws in the finite, infinite, and infinitesimal and even for sets with parts of different dimensions. The real numbers cannot fill the number line because of gaps between them. The sets, fuzzy sets, multisets, and set operations express and form not all collections. Infinity is a heap of very different infinities the cardinality only can very roughly discriminate and no tool can exactly measure. Operations are considered for natural numbers or count-

able sets of operands only. In each concrete (mixed) physical magnitude, e.g. 5 liter fuel, there is no known operation unifying "5 L" and "fuel". The absolute error is noninvariant. The relative error applies to the simplest formal equalities of two numbers only and even then is ambiguous and can be infinite. Measurement theory leads to losing information via artificially limiting precision and ignoring systematic errors, as well as to precision illusions. Let us $10^6$ times measure a bolt length (of 5.3 cm unknown for us) via a ruler of 100 cm length with centimeter divisions. Then $10^6$ times we obtain exactly 5 cm and the same mean with its illusive quadratic mean error $0.5/3^{1/2}$ cm$/(10^6)^{1/2} < 3 * 10^{-3}$ mm (and the same precision by measuring the length of a large hall with building errors of at least 1 cm). There is no weighting a posteriori possibly equiprecise data a priori via using their already available errors.

Universal physics [3, 4] including material unistrength introduces invariant and universal dimensionless physical quantities such as ion implantation unidoses and mechanical unistresses. They provide for the first time discovering universal strength laws of nature. They hold for any anisotropic materials with different resistance to tensions and compressions and for any variable loads with possibly rotating the principal directions of the stress state at a point of such a material during loading.

Universal mathematics [3, 5] provides the uninumbers generalizing the real numbers via including some infinite cardinal numbers as canonic positive infinities and signed zeroes reciprocals as canonic overinfinities. Include, e.g., ω (the first Cantorian cardinal $\aleph_0$) and Ω (the continuum cardinality $\mathfrak{C}$). Quantification builds algebraically quantioperable quantielements ${}_q a$ (e.g. ${}_{5\ L}$fuel) and quantisets $\{{}_{q(j)}a(j) \mid j \in J\}$ with any quantity $q(j) = q_j$ of each element $a(j) = a_j$ which both are any objects indexed via any (possibly uncountable) index set J. Quantiset uniquantities $Q = \Sigma_{j\in J}\, q_j$ are universal, perfectly sensitive, and even uncountably algebraically additive measures with universal conservation laws. Canonic sets interpret canonic positive infinities, e.g. via $Q(N) = Q\{n \mid n \in N = \{1, 2, 3, \ldots\}\} = \omega$ and $Q]0, 1] = Q\{r \mid r \in R\ ,\ 0 < r \le 1\} = \Omega$ (R the reals). In created uniarithmetics, quantialgebra, and quantianalysis of the finite, the infinite, and the overinfinite with quantioperations and quantirelations, the uninumbers evaluate, precisely measure, and are interpreted by quantielements and quantisets with uniquantities. Then, e.g., $Q\{a + bn \mid n \in N\} = \omega/|b| - a/b - 1/2 + 1/(2|b|)$, $Q]a\ ,\ b[^n = ((b - a)\Omega - 1)^n$, and $Q(R^n) = 2^n\omega^n\Omega^n$ $(a\ ,\ b \in R)$. They provide adequately setting and solving many typical urgent problems. The unierror corrects and generalizes the relative error. The unireserve, unireliability, and unirisk additionally estimate exact objects, models, and solutions by exactness confidence.

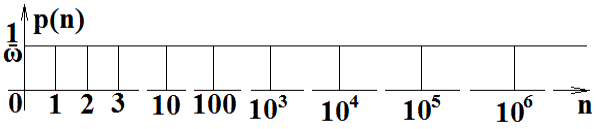


**Figure 4.7 Probability of selecting any n∈N**

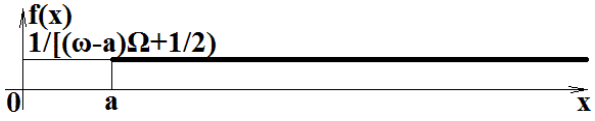


**Figure 4.8 Probability density f(x) for [a, ∞)**

Universal metrology [3] adequately sets and analytically solves nontrivial general and specific metrological problems. Their solutions provide adequately determining the true values of measured quantities with eliminating averaging and partition errors and exactly expressing any uninumber (Figure 4.7Figure 4.8). Temporary overprecision (e.g. 5 cm, 5.33 cm, … in that bolt measurement) excludes losing measurement information. Reducing the end result precision to the instrument precision (e.g. giving 5 cm or in the best case 5.3 cm in that bolt length measurement) excludes precision illusions.

Unimetrology creates fundamentally new opportunities in measurement by great data scatter, e.g. in aeronautical fatigue, to discover new phenomena and laws of nature.

**References:**

[1] Encyclopaedia of Mathematics. Ed. Michiel Hazewinkel. Volumes 1 to 10. Supplements I to III. Kluwer Academic Publ., Dordrecht, 1987-2002

[2] Encyclopaedia of Physics. Chief Ed. Siegfried Flügge. Springer, Berlin, 1973 etc.

[3] Lev Gelimson. Elastic Mathematics. General Strength Theory. The "Collegium" All World Academy of Sciences Publishers, Munich, 2004

[4] Lev Gelimson. Providing Helicopter Fatigue Strength: Unit Loads. In: Structural Integrity of Advanced Aircraft and Life Extension for Current Fleets – Lessons Learned in 50 Years After the Comet Accidents, Mechanical and Physical Journal of the 23rd ICAF Symposium, Claudio Dalle Donne (Ed.), 2005, Hamburg, Vol. II, 589-600

[5] Lev Gelimson. Providing Helicopter Fatigue Strength: Flight Conditions. In: Structural Integrity of Advanced Aircraft and Life Extension for Current Fleets – Lessons Learned in 50 Years After the Comet Accidents, Proceedings of the 23rd ICAF Symposium, Claudio Dalle Donne (Ed.), 2005, Hamburg, Vol. II, 405-416

## 4.5 Universal Probabilistic Science

*Lev G. Gelimson (AICFS)*

Measurement data processing is based on classical probability theory [1]. It simply postulates the existence of at most countably additive probability between 0 for impossible events and 1 for certain events. But probability $p_n = p$ of selecting certain $n \in N = \{1, 2, ...\}$ does not exist. In any continual set, the probabilities to take distinct values are regarded as the same (zero) but with different probability densities and no possibility to obtain required 1 as the sum. Probability densities f(x) with formal derivative sense can exceed 1 and are no probabilities. Then the maximum likelihood principle has no clear sense. There are no perfectly sensitive universal measure with conservation laws and no commeasure for discrete and continual parts of a mixed distribution. The quadratic mean error leads to the illusion that the arithmetic mean is the most probable value by strongly asymmetric distributions with great skewness. Noninteger-order and infinite moments do not exist at all. The variance, higher-order moments, and the least square method too strongly magnify the inputs of data with great errors by reducing the roles of the most precise data. Real samples are given predefined distributions. The typical normal distribution symmetrizes and infinitizes the binomial distribution with adequately fitting it near its maximum and p = 0.5 only.

Universal mathematics [2-5] provides the uninumbers. In them, universal probabilistic science gives $p_n = p = \omega$ (the first Cantorian cardinal $\aleph_0$), and an n-dimensional probability with probability density f(x) is simply $f(x)/\Omega^n$ ($\Omega$ the continuum cardinality $\mathfrak{C}$). In the axioms system, a random variable is a quantiset of values with uncountably additive nonnegative uninumber quantities which are pointwise probabilities to take these values and with unit uniquantity. Possibly uncountably quantiunifying random variables uses unifying their sets of values with averaging their probabilistic quantities of the same values. Suitably operable pointwise probability distribution functions g(x) provide adequately regarding typical sample distribution skewness (Figure 4.9Figure 4.10).

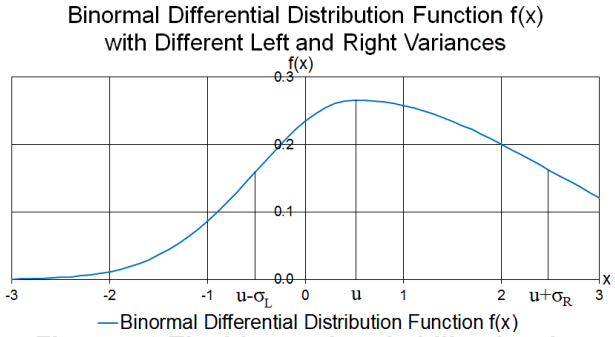


**Figure 4.9 The binormal probability density**

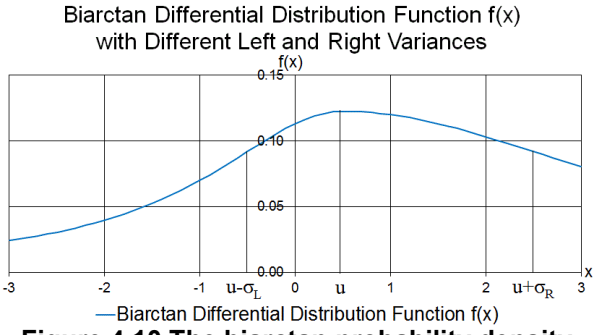


**Figure 4.10 The biarctan probability density**

Apply the maximum likelihood principle to f(x) = Ωg(x) by possibly asymmetric sample distributions of random variables (and their values) $x_1 \le x_2 \le \dots \le x_n$ with generally different left and right variances $\sigma_{Li}^2$ and $\sigma_{Ri}^2$ via $f_i(x)$, as well as $\sigma_L^2$ and $\sigma_R^2$ for total f(x) asymmetric even by symmetric $f_i(x)$ (i = 1, 2, … , n). Quantiunifying binormal distributions provides general analytical solution giving by $\sigma_{Li}^2 = \sigma_{Ri}^2$ unimode u via

$$u = \Sigma_1^n x_i/n - \Sigma_{x(i)\le u} (x_i-u)\{1 - \exp[-(x_i-u)^2/(2\sigma_L^2)]\}/n - \Sigma_{x(i)\ge u} (x_i-u)\{1-\exp[-(x_i-u)^2/(2\sigma_R^2)]\}/n,$$
$$\sigma_L^2 = \Sigma_{x(i)\le u} (x_i - u)^2 \exp[-(x_i - u)^2/(2\sigma_L^2)] / \Sigma_{x(i)\le u} \exp[-(x_i - u)^2/(2\sigma_L^2)],$$
$$\sigma_R^2 = \Sigma_{x(i)\ge u} (x_i - u)^2 \exp[-(x_i - u)^2/(2\sigma_R^2)] / \Sigma_{x(i)\ge u} \exp[-(x_i - u)^2/(2\sigma_R^2)]$$

using intelligent iteration. Alternative sign-conserving multiplication $"\Pi_{j\in J} a_j = \min(\text{sign } a_j \mid j \in J) |\Pi_{j\in J} a_j|$ provides alternative base sign conserving exponentiation $a"^b = |a|^b$ sign a for negative bases and hence unrestricted power and exponential functions, e.g. moments of any (e.g. non-integer) orders. Universal probabilistic science includes general theories of efficiently utilizing a posteriori weighting a priori equiprecise data, of asymmetrizing classical and introduced distributions, of efficiently determining unimodes with really maximum probabilities, and of analytizing tabular functions.

Universal probabilistic science provides scientific fundament for universal statistical science and universal data processing science. Their theories and methods of setting and solving many typical urgent problems including data processing even by great data scatter give adequate and correct results, e.g. in aeronautical fatigue.

**References:**

[1] Selected Works of A. N. Kolmogorov. 3 Volumes. Dordrecht, Kluwer Academic Publishers, 1991-1993. Volume II. Probability Theory and Mathematical Statistics

[2] Lev Gelimson. Quantianalysis: Uninumbers, Quantioperations, Quantisets, and Multiquantities (now Uniquantities). Abhandlungen der WIGB (Wissenschaftlichen Gesellschaft zu Berlin), 3 (2003), Berlin, 15-21

[3] Lev Gelimson. Elastic Mathematics. General Strength Theory. The "Collegium" All World Academy of Sciences Publishers, Munich, 2004

[4] Lev Gelimson. Providing Helicopter Fatigue Strength: Flight Conditions. In: Structural Integrity of Advanced Aircraft and Life Extension for Current Fleets – Lessons Learned in 50 Years After the Comet Accidents, Proceedings of the 23rd ICAF Symposium, Claudio Dalle Donne (Ed.), 2005, Hamburg, Vol. II, 405-416

[5] Lev Gelimson. Corrections and Generalizations of the Least Square Method. In: Review of Aeronautical Fatigue Investigations in Germany during the Period May 2007 to April 2009, Ed. Dr. Claudio Dalle Donne, Pascal Vermeer, CTO/IW/MS-2009-076 Technical Report, International Committee on Aeronautical Fatigue, ICAF 2009, EADS Innovation Works Germany, 2009, 59-60.

### 4.6 Universal Statistical Science

*Lev G. Gelimson (AICFS)*

Measurement data processing is based on classical probability theory with its defects and on mathematical statistics [1]. It mixes equiprecise a priori but nonequiprecise data a posteriori without adequately weighting. Finite samples with skew distributions are given predefined infinite symmetric distributions with proper approximation near maximums only. Using the quadratic mean error and the arithmetic mean m (as the expectation) only leads to the illusion that this mean is the most probable value also by strongly asymmetric distributions with great skewness. Classical statistics either overestimates or subjectively ignores outliers and leads to results instability. Regression analysis gives the least square method results different by mutually replacing the variables roles and only qualitatively proves the fact of dependence via rejecting the null hypothesis (full independence) without estimating errors and improving formulae. Tabular data only provide neither analytical nor computational operability. There is no polymethodicity with results comparison and adequacy test.

Universal statistical science [2, 3] uses base sign conserving exponentiation $a"^b = |a|^b$ sign a for negative bases in universal mathematics. Moments and absolute moments

$$^{s|t}M_y = \Sigma_{i=1}^{n} w_i^s (x_i - y)"^t / \Sigma_{i=1}^{n} w_i^s, \; ^{s|t}|M|_y = \Sigma_{i=1}^{n} w_i^s |x_i - y|^t / \Sigma_{i=1}^{n} w_i^s$$

of any (possibly noninteger) orders s and t with adequately weighting a posteriori equiprecise data a priori $x_i$ with positive weights $w_i$ where y may be, e.g., exact value $x_0$ , mean m , or unimode u for which $\Sigma_{i=1}^{n} w_i (x_i - u)"^t = 0$ are very efficient.
Signed power mean and s|t-standard deviation of a single data by known $x_0$ are

$$^{s|t}m_y = y + [\Sigma_{i=1}^{n} w_i^s (x_i - y)"^t / \Sigma_{i=1}^{n} w_i^s]"^{1/t}, \; ^{s|t}\sigma_x = [\Sigma_{i=1}^{n} w_i^s |x_i - x_0|^t / \Sigma_{i=1}^{n} w_i^s]^{1/t}.$$

Properly weighting asymmetric sample distributions with introduced asymmetry grade $A = (\sigma_R - \sigma_L)/(\sigma_R + \sigma_L)$ can be based on different left and right standard deviations $\sigma_L$ and $\sigma_R$ by values $x_1 \le x_2 \le \ldots \le x_n$ or their numbers. Also to asymmetric populations apply, e.g., the weights corresponding to binormal, biarctan, or binomial distributions

$$w_i = \exp[-(x_i - u)^2/(2\sigma_L^2)], \; \sigma_L^2 = \Sigma_{x(i)\le u} (x_i - u)^2/\Sigma_{x(i)\le u} 1 \text{ by } x_i \le u ,$$
$$w_i = \exp[-(x_i - u)^2/(2\sigma_R^2)], \; \sigma_R^2 = \Sigma_{x(i)\ge u} (x_i - u)^2/\Sigma_{x(i)\ge u} 1 \text{ by } x_i \ge u ;$$
$$w_i = 1/[1 + (x_i - u)^2/(3\sigma_L^2)] \text{ by } x_i \le u , \; w_i = 1/[1 + (x_i - u)^2/(3\sigma_R^2)] \text{ by } x_i \ge u ;$$
$$w_i = (n-1)!/[\Gamma(h)\Gamma(n - h + 1)] \, p^{h-1}(1 - p)^{n-h}, \; h(i) = 1 + (n-1)(x_i-x_1)/(x_n-x_1), \; p=(h_{med}-1)/(n-1),$$
$$w_i = (n - 1)!/[(i - 1)!(n - i)] \, p^{i-1}(1 - p)^{n-i}, \text{ or simply } w_i = (n - 1)!/[(i - 1)!(n - i)].$$

Universal statistical science applies to the classical Cavendish data [4] (Figure 4.11Figure 4.12).

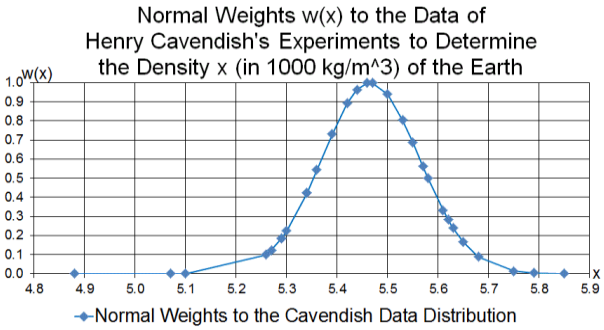


**Figure 4.11 Weights to Cavendish's data**

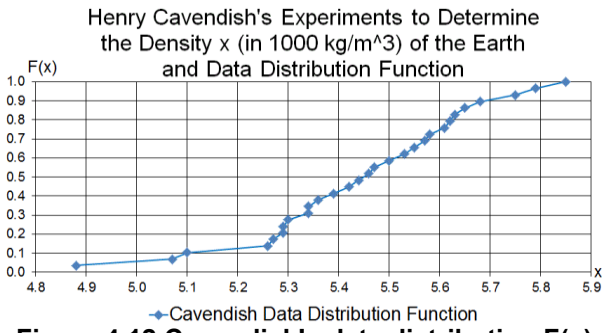


**Figure 4.12 Cavendish's data distribution F(x)**

The modern value for the Earth density in $10^3$ kg/m$^3$ is ρ = 5.51 and for the Newtonian constant of gravitation in $10^{-11}$ m$^3$ kg$^{-1}$ s$^{-2}$ G = 6.674 based on the reported data between 6.672 and 6.676 [5]. Using Cavendish's 29 data, classical statistics gives ρ = m = 5.448 with standard deviation $\sigma_\rho$ = 0.22 and G = 6.752; universal statistical science gives ρ = u = 5.466 with deviations ${}^u\sigma_L$ = 0.096, ${}^u\sigma_R$ = 0.097, and G = 6.729. Using Cavendish's 23 data after changing a wire via a stiffer wire, classical statistics gives ρ = m = 5.483 with standard deviation $\sigma_\rho$ = 0.19 and G = 6.708 but using median $m_{ed}$ = 5.46 and following Charlier [1] u = 3$m_{ed}$ - 2m = 5.414 and G = 6.794 whereas universal statistical science gives ρ = u = 5.49 with deviations ${}^u\sigma_L$ = 0.10, ${}^u\sigma_R$ = 0.12, G = 6.700. Therefore, applying universal statistical science to the classical Cavendish data gives new results for the Newtonian constant of gravitation.

Universal statistical science provides scientific fundament for universal data processing science. Their theories and methods of setting and solving many typical urgent problems including data processing even by great data scatter, asymmetry, skewness, and outliers give adequate and correct results, e.g. in aeronautical fatigue.

**References:**

[1] H. Cramér. Mathematical Methods of Statistics. Princeton University Press, 1945

[2] Lev Gelimson. Elastic Mathematics. General Strength Theory. The "Collegium" All World Academy of Sciences Publishers, Munich, 2004

[3] Lev Gelimson. Providing Helicopter Fatigue Strength: Flight Conditions. In: Structural Integrity of Advanced Aircraft and Life Extension for Current Fleets – Lessons Learned in 50 Years After the Comet Accidents, Proceedings of the 23rd ICAF Symposium, Claudio Dalle Donne (Ed.), 2005, Hamburg, Vol. II, 405-416

[4] Henry Cavendish. Experiments to Determine the Density of the Earth. Philos. Transactions of the Royal Society. London, 88, 1798

[5] Peter J. Mohr, Barry N. Taylor, and David B. Newell. CODATA Recommended Values of the Fundamental Physical Constants: 2010. National Institute of Standards and Technology, Gaithersburg, Maryland, USA, 2012

## 4.7 Universal Data Processing Science with Multiple-Sources Intelligent Iteration

*Lev G. Gelimson (AICFS)*

Modern data processing is based on classical probability theory and statistics [1] with their defects. Regression analysis gives the least square method results different by mutually replacing the variables roles and only qualitatively proves the fact of dependence via rejecting the null hypothesis of full independence. There are no adequately estimating the errors of the dependence formula and no improving it. Single-source iteration has an inflexible algorithm often with very slow convergence.

Universal data processing science [2-4] includes a number of corresponding theories.
Direct equiprecise measurement theory proves that for groups i (i = 1, 2, … , n) of data $x_{ij}$ (j = 1, 2, … , k(i) = $k_i$), the variance of a separate data by known exact value a

$$\sigma_x^2 = \Sigma_{i=1}^n \Sigma_{j=1}^{k(i)} (x_{ij} - a)^2 / \Sigma_{i=1}^n k(i) = \{\Sigma_{i=1}^n k(i) \Sigma_{j=1}^{k(i)} [(x_{ij} - a)^2 / k(i)]\} / \Sigma_{i=1}^n k(i)$$

is groupwise invariant. The same holds for the general mean value

$$m = \Sigma_{i=1}^n \Sigma_{j=1}^{k(i)} x_{ij} / \Sigma_{i=1}^n k(i) = [\Sigma_{i=1}^n k(i) \Sigma_{j=1}^{k(i)} x_{ij} / k(i)] / \Sigma_{i=1}^n k(i)$$

(replacing a) if and only if either the dependence of m on $x_{ij}$ with the Bessel formula is ignored and $\Sigma_{i=1}^n k(i)$ rather than $\Sigma_{i=1}^n k(i) - 1$ is used in the last denominator or this subtracting 1 also applies to the group weights k(i) - 1 instead of k(i):

$$\sigma_x^2 = \Sigma_{i=1}^n \Sigma_{j=1}^{k(i)} (x_{ij} - m)^2 / [\Sigma_{i=1}^n k(i) - 1]$$
$$= \{\Sigma_{i=1}^n [k(i) - 1] \Sigma_{j=1}^{k(i)} (x_{ij} - m)^2 / [k(i) - 1]\} / [\Sigma_{i=1}^n k(i) - 1].$$

For groupwise noninvariant variances $\sigma_{x(i)}^2$ about groupwise mean values m(i),

$$\sigma_x^2 = \{\Sigma_{i=1}^n [k(i) - 1] \sigma_{x(i)}^2 + \Sigma_{i=1}^n k(i) m(i)^2 - \Sigma_{i=1}^n k(i) m^2\} / [\Sigma_{i=1}^n k(i) - 1].$$

Direct nonequiprecise measurement theory gives weights $p_i k_i/\sigma_{x(i)}^2$ to data means $x_i$ with variances $\sigma_{x(i)}^2$ and finally for weighted arithmetic mean m and its variance $\sigma_m^2$

$$m = \Sigma_{i=1}^n w_i k_i/\sigma_{x(i)}^2 x_i / \Sigma_{i=1}^n w_i k_i/\sigma_{x(i)}^2, \sigma_m^2 = 1 / \Sigma_{i=1}^n w_i k_i/\sigma_{x(i)}^2.$$

Unimode theory introduces unimode u (unlike the discrete or descriptive mode) as the most probable value which generalizes the continuous distribution mode. The weighted power unimode method gives for t > 0 equation $\Sigma_{i=1}^n w_i (x_i - u)^{"t} = 0$ with using base sign conserving exponentiation $a^{"b} = |a|^b$ sign a . By $x_1 \le x_2 \le \dots \le x_n$ , apply asymmetric distributions with different left and right variances $\sigma_L^2$ and $\sigma_R^2$.

Extreme data maximum and mean correction theories without ignoring outliers least-correct the equal amounts of both the least and the greatest data so that their distances from the next data do not exceed the maximum or the mean distance for the remaining data, respectively, e.g. by the classical Millikan data [5] (Figure 4.13Figure 4.14).

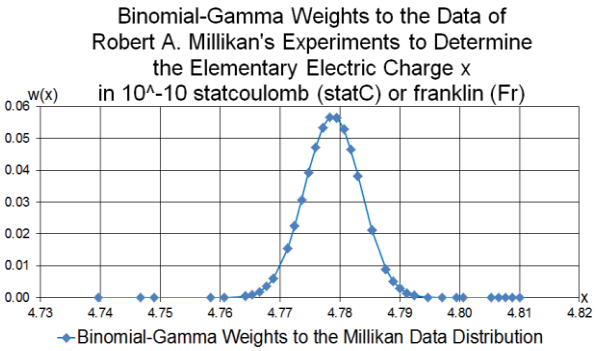


**Figure 4.13 Weights w(x) to Millikan's Data**

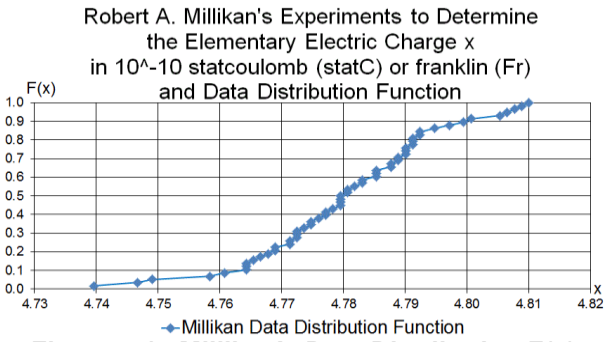


**Figure 4.14 Millikan's Data Distribution F(x)**

Multiple-sources iteration theory rationally introduces additional initial sources.
Intelligent iteration theory rationally replaces each already calculated iteration approximation with an absolutely freely chosen pseudosolution to a general problem.

The modern value for the elementary charge in $10^{-10}$ statcoulomb is e = 4.8032. Using Millikan's 58 data, classical statistics gives e = m = 4.7806 with standard deviation $\sigma_e$ = 0.0147 but using median $m_{ed}$ = 4.7801 and following Charlier [1] u = $3m_{ed}$ - 2m = 4.7791. Universal data processing science gives e = u = 4.784 with deviations ${}^{u}\sigma_L$ = 0.0053 and ${}^{u}\sigma_R$ = 0.0050. Therefore, applying this science to the classical Millikan data gives new results for the elementary charge as one of the fundamental physical constants. This also shows that it is very important to publish the complete experimental data and not only the final results of their statistical processing because new theories and methods can essentially improve the results.

Universal data processing science and multiple-sources intelligent iteration give correct results by data scatter, asymmetry, and outliers, e.g. in aeronautical fatigue.

**References:**

[1] H. Cramér. Mathematical Methods of Statistics. Princeton University Press, 1945

[2] Lev G. Gelimson. General Problem Theory. Abhandlungen der WIGB (Wissenschaftlichen Gesellschaft zu Berlin), 3 (2003), Berlin, 26-32

[3] Lev Gelimson. Elastic Mathematics. General Strength Theory. The "Collegium" All World Academy of Sciences Publishers, Munich, 2004

[4] Lev G. Gelimson. Providing Helicopter Fatigue Strength: Flight Conditions. In: Structural Integrity of Advanced Aircraft and Life Extension for Current Fleets – Lessons Learned in 50 Years After the Comet Accidents, Proceedings of the 23rd ICAF Symposium, Claudio Dalle Donne (Ed.), 2005, Hamburg, Vol. II, 405-416

[5] Robert A. Millikan. On the Elementary Electric Charge and the Avogadro Constant. Phys. Rev., 2 (2), 1913, 109-143

# 5 Fatigue and Fracture of Metallic Aerostructure Materials

## 5.1 Enhanced Fatigue and Damage Tolerance of Aircraft Components by Introduction of Residual Stresses – A Comparison of Different Processes

*E. Hombergsmeier, U. C. Heckenberger, V. Holzinger (EADS IW) D. Furfari (Airbus)*

Highly loaded aircraft components have to fulfill strict fatigue and damage tolerance requirements. To reach these requirements especially at critical locations additional treatments might be necessary. One of these possibilities is the local introduction of beneficial residual stresses. A standard and well qualified process to introduce compressive residual stresses is Shot Peening (SP). Alternative and more advanced treatments are Ultrasonic Shot Peening (USP) and Laser Shock Peening (LSP). Laser Shock Peening is a mechanical process capable to introduce deep compressive residual stresses into the surface of a metallic component. Ultrasonic Peening is a modification of the Shot Peening process where the balls are accelerated by ultrasound. By means of Laser Shock Peening the residual compressive stress field can extend deeper below the treated surface than that produced by conventional or Ultrasonic Shot Pening (i.e. with steel or ceramic balls). The effect of such deep compressive stress profile results in a significantly greater benefit in fatigue resistance and reduced crack propagation after Laser Shock Peening compared to both Shot Peening variations.

### Laser Shock Peening (LSP)

LSP (see Figure 5.1) imparts a layer of beneficial compressive residual stresses underneath the surface of metal components to help them better resist the detrimental effects of fatigue. This has obvious benefits for extending the service life of metallic components at the manufacturing stage but it may also be possible to apply this technique to in-service aircraft to extend the service goals of existing structures. Degradation processes, such as fatigue, limit service lives of aircraft structures. Technologies and methodologies that improve the resistance of structures to these degradation processes are of benefit to industry in terms of extending the service life of the structure and reducing maintenance costs. In addition to the improvement of the manufacturing methods, which would directly impact on quality improvement and cost reduction, it is necessary to investigate these technologies in view of increasing operational costs, for example, extending maintenance intervals by enhancing metals performance.

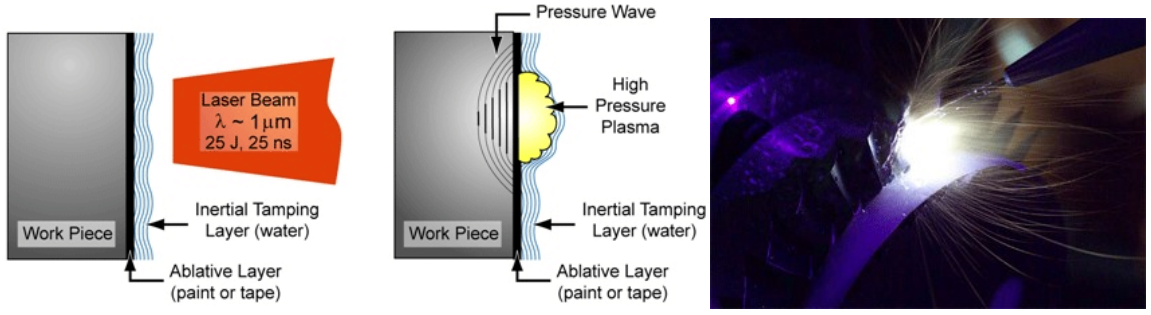


**Figure 5.1 Sketch and photograph of Laser shock peening process [source: MIC – Metal Improvement Company].**

**Shot Peening (SP and USP)**

Ultrasonic Shot Peening (USP) application (see Figure 5.2 b) is used to improve fatigue life, resistance to stress corrosion cracking and fretting fatigue. This surface impact treatment solution is done by throwing beads on a specific area of the part to be peened. It introduces beneficial compressive residual stresses which guarantee an increased life time. Ultrasonic Shot Peening technology allows the use of high quality beads. Quality beads combined to the real-time control of parameters, ensures a repeatable and efficient treatment. Ultrasonic Shot Peening (USP) induces a low roughness and a better surface quality compared to the conventional shot peening (see Figure 5.2 a). This has a direct influence on fatigue-life enhancement.

**Experimental Approach**

The Laser Peening and the Shot Peeening processes are applicable to a range of aerospace alloys (Ti, AL or Steel) and this programme aims to understand benefits (improved fatigue life) of applying the SP, USP and LSP processes to typical airframe structures made of high strength Al alloy (7xxx series) with “heavy” gauges (i.e. thickness greater than 30 mm). It is therefore essential and a challenge to investigate the influence of engineered residual stresses on metallic materials used in aircraft structures (e.g. Aluminium alloys).

**Fatigue improvement**

Fatigue investigations are performed on notched specimens made of 7xxx aluminium plate material. For comparison the specimens are tested in four different conditions: milled, Shot Peened according to Airbus specification by MIC Unna, Ultrasonic Shot Peened by SONATS, Nantes and Laser Shock Peened by MIC Earby.

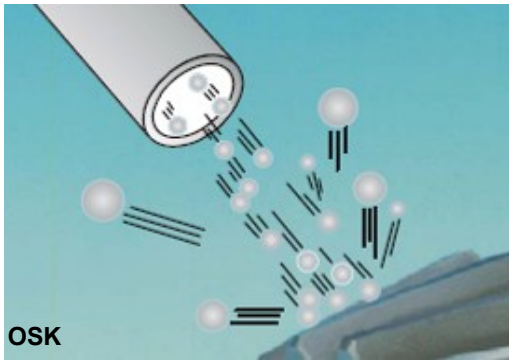


a) conventional shot peening

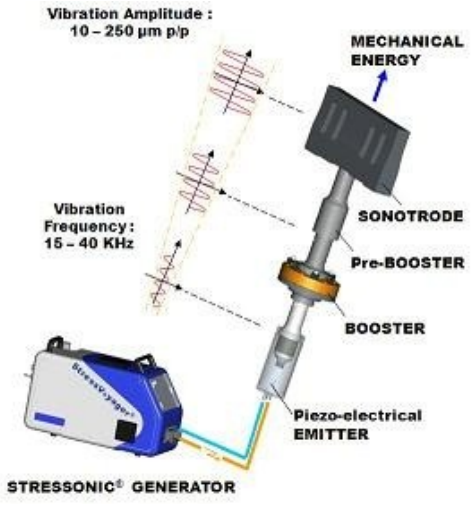


b) ultrasonic shot peening by SONATS

**Figure 5.2 Principle of shot peening processes.**

Due to superposition of compressive residual stresses onto the tensile stresses generated during cyclic fatigue, crack propagation is suppressed if the net stresses remain in the compressive state. Therefore a significant improvement of the fatigue life was found for an R ratio of 0.1 and

even for -1.75. Shot Peening leads to a fatigue improvement of about 60 % for the CAA treated specimens shown in Figure 5.3. For the same specimen geometry a fatigue life improvement of 100 %, depending on the load level, can be obtained through laser shock peening (Figure 5.3a). However not only for the positive R ratio, where it is quite obvious, but also for the negative R ratios, R = -1.75 a slightly lower, but still significant increase of the fatigue life is generated by shot peening and laser shock peening (Figure 5.3 b). This positive effect of the laser shock peening treatment on the fatigue behaviour can be explained by the much deeper residual stress profile in comparison to shot peening, created by the LSP process.

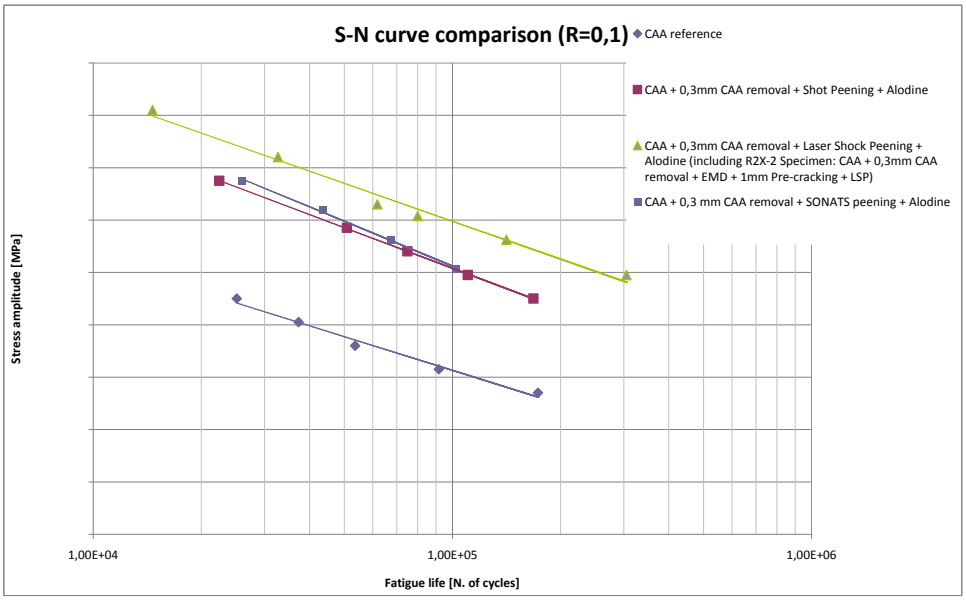


a) R ratio 0.1

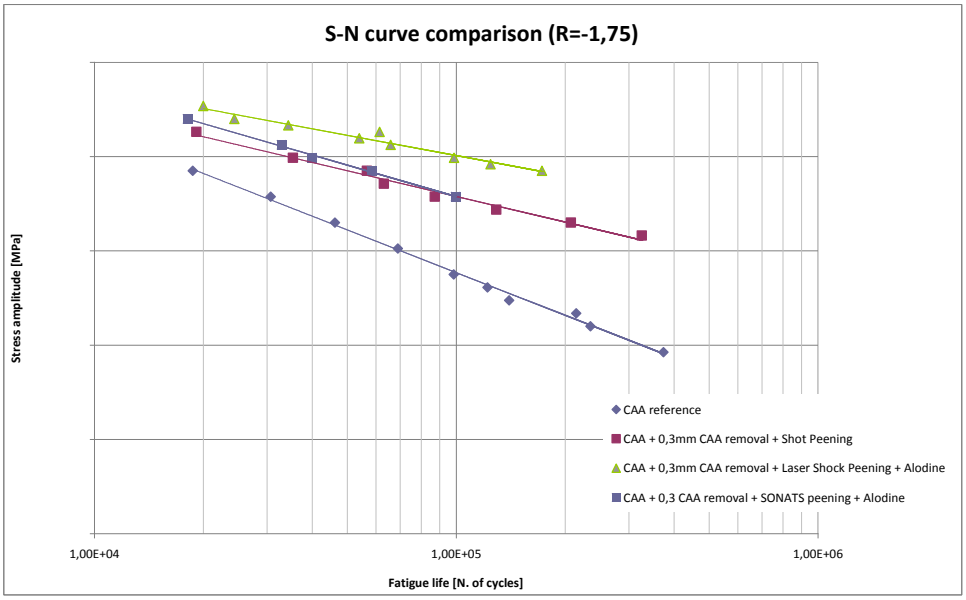


b) R ratio -1.75

**Figure 5.3 S/N-curve for different surface conditions and R-ratios**

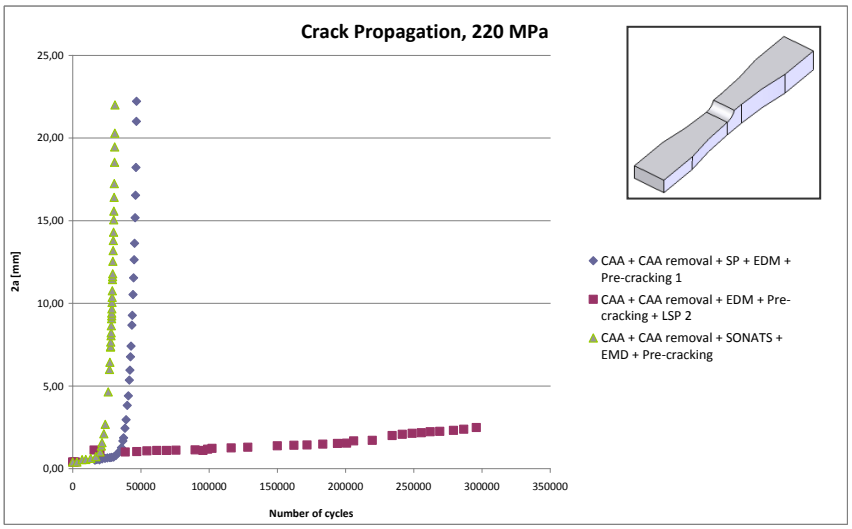


**Figure 5.4 Crack propagation curve for different processes to introduce residual stresses**

Similarly to the improved high cycle fatigue behaviour the crack propagation rate was significantly reduced due to the compressive residual stress field. Using the same maximum stress the fatigue pre-crack of the LSP specimens could be hardly increased whereas the SP and USP specimen showed continuous crack propagation (Figure 5.4). Therefore this process has tremendous potential for the mitigation of otherwise life-limiting surface cracking, especially if applied to the airframe at critical locations where the conventional methods (e.g. shot peening) would have very limited benefit.

## 5.2 Fatigue Behavior of Additive Manufacturing Parts

*D. Greitemeier, K. Schmidtke, V. Holzinger and C. Dalle Donne (EADS IW)*

Additive Manufacturing is increasingly considered for manufacturing high quality aerospace parts. Therefore it is essential to cover the full range of material characterisations. Today this characterization is at an early stage especially regarding fatigue loads. Only few data are available. In frame of the maturation of the technology readiness in EADS a program on mechanical behavior of additive manufactured Ti-6Al-4V was carried out. More particularly static strength, fracture toughness and high cycle fatigue strength were investigated.

The dots in Figure 5.6correspond to S-N experiments carried out with machined Ti-6Al-4V specimens made in an powder bed electron beam machine (PP-EB). The sizes and shapes of crack nucleating defects were determined microscopically on the fracture surfaces of all tested PB-EB specimens. Cracks were typically nucleated at defects near the surface.

S-N curve calculations with AFGROW were carried out with a virtual specimen containing a single initial flaw which corresponded to the smallest and biggest detected defect,Figure 5.5. Simulation based on a fracture mechanical approach seems to be a suitable method for life prediction of PB-EB Ti-6Al-4V.

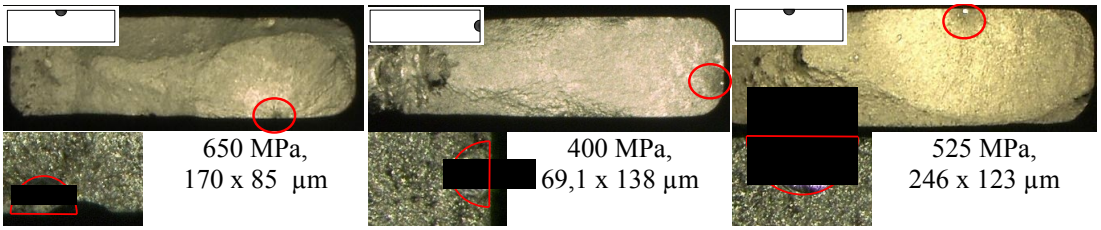


**Figure 5.5 Fracture surfaces of PB-EB specimens**

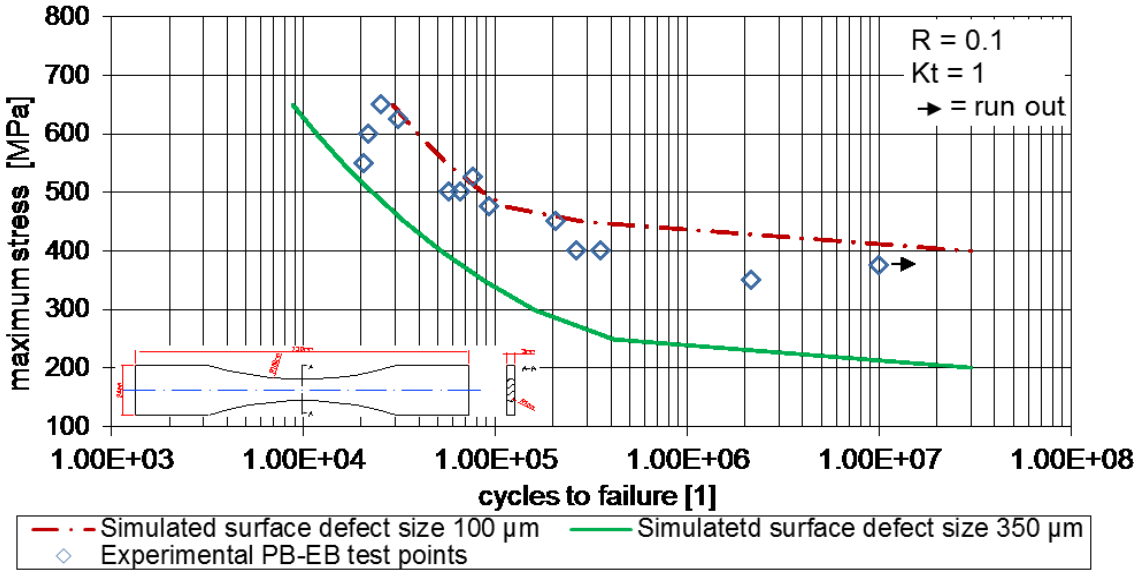


**Figure 5.6 Comparison of experimental and simulated S-N results.**

# 6 Fatigue and Fracture of Composites

## 6.1 Simulation of lap-shear fracture test of hybrid metal/CFRP laminatesStructu

*P. Naghipour, K. Schulze, M. Bartsch, J. Hausmann, J. Schneider (DLR-WF)*

Hybrid metal/CFRP laminates are considered for aerospace structural applications since by combining both material classes it is possible to utilize the advantageous properties of both and overcoming their weaknesses. In metal/CFRP hybrid laminate architectures, the metal fraction improves the impact resistance, and metal layers at the outer surface protect the CFRP core from environmental effects, such as ultraviolet radiation, moisture, and abrasive wear. CFRP provides high strength and high stiffness along with low weight. However, the interface between metal and CFRP implicates a higher complexity than interfaces between similar materials. E.g. differences in stiffness lead to shear stresses at free edges promoting delamination fracture. A test configuration considered for characterizing resistance against interfacial fracture is the lap shear test, which is not standardized for hybrid laminates. In order to assure the validity of experimental results, the effects of the chosen specimen geometry and experimental setup has been comprehensively investigated by means of experiments and numerical analyses.

Hybrid Al/CFRP laminates investigated in this study consist of alternating aluminium/CFRP plies. Three plies of aluminium (EN AW-6016, 0.5 mm thick), and two 4-ply CFRP layups with 0.14 mm ply thickness, with a polyamide (PA66) matrix and a fibre volume fraction of 47%, were stacked to build up the hybrid laminate. The composite layer was made of UD tape with fibre orientation parallel to the mechanical load in the test. The specimen was notched in order to subject the selected interface to the applied load (Figure 6.1 a).

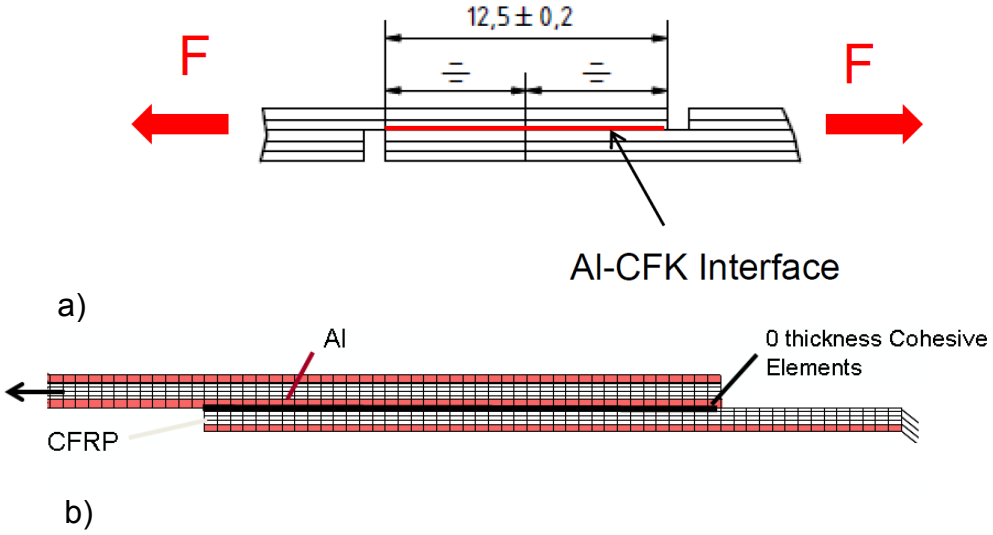


**Figure 6.1 Hybrid metal/CFRP specimen for lap shear testing a) schematic of the notched specimen and b) Finite Element Model of the lap shear joint.**

Although, in real applications the electrochemical corrosion of aluminium in contact with carbon fibres needs to be considered it is neglected in this study. Therefore, further developments are necessary to protect the aluminium from corrosion. The hybrid laminates were produced by Technical University of Chemnitz within a joint project funded by German Research Foundation (DFG). The test machine used was a 10 tons Instron testing machine equipped with a 100 kN load cell to measure the load for lap shear fracture. The cross-head displacement rate was set to 1.0 mm/min.

The numerical model is sketched in Figure 6.1 b and comprised damageable plies for CFRP, user defined interface elements in between CFRP and aluminium layer, and an elastic–plastic metal layer. An in-built ply damage model in ABAQUS [1], partially based on the works of Hashin [2] and Matzenmiller et al. [3], is used to define the intra-laminar ply damage behaviour. The interface damage is represented by user-defined cohesive elements, the constitutive mathematical model of which is a combination of the cohesive models proposed by Camanho et al. [4] and Ortiz and Pandolfi [5], with two major improvements. First, the model proposed in [4] is further enhanced by utilising quadratic cohesive elements, and next the highly non-linear cohesive behaviour (bilinear behaviour) is further smoothed by the exponential softening law suggested in [5].

Input data used for modelling the individual CFRP (CF-PA66) lamina are taken from literature [6]. Some material parameters for the cohesive elements have to be obtained through mixed mode bending (MMB) experiments [7]. As it was not possible to conduct MMB experiments in the project timeline, all interface properties were estimated from available values in literature [8], and calibrated via lap shear experimental results. First and second mode interfacial fracture energies and initial interfacial strengths of the hybrid interface are assumed to vary between 40% and 60% of the corresponding pure CFRP interface values (postulating 20% of uncertainty range for these parameters), as a non-homogeneous interface is always weaker than a homogeneous one. When material parameters of the hybrid interface are taken as 40% of the pure CFRP values, a good approximation of the lap shear failure load is attained (Figure 6.2a).

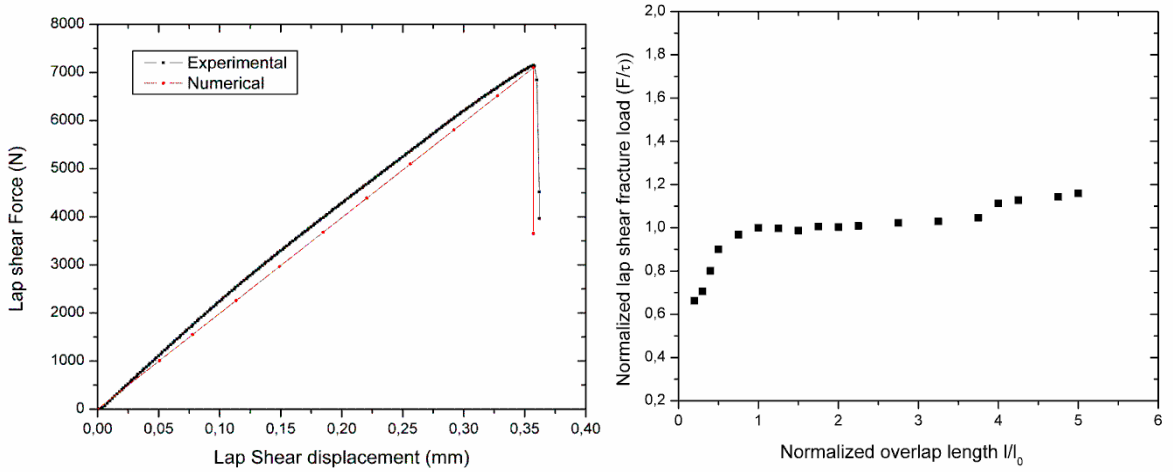


**Figure 6.2 Results: a) Comparison of experimental and simulated load-displacement curve and b) influence of normalized overlap length on normalized shear fracture load.**

A numerical parametric study is conducted to investigate the effect of specimen geometry on load–displacement results. While the total length/width of the specimen does not have a sensible effect on the maximum force, the lap shear fracture strength is sensitive on overlap length variations for short overlap lengths, compare Figure 6.2b.

By means of the experimentally validated numerical analyses the specimen design for lap shear tests of hybrid laminated could be confirmed, and the conditions for generating valid experimental results have been explored.

This study was conducted in the frame of the joint project ‘‘3HSL – Hybride, hochsteife und hochfeste Schichtverbunde für großseriennahe Anwendungen im Leichtbau’’. The funding by the German Research Fundation (DFG) under project number PAK413-1 is acknowledged.

**References**

[1] Hibbitt, Karlsson, Sorensen. ABAQUS 6.6 User’s Manuals. Pawtucket, USA; 1996.

[2] Hashin Z. Failure criteria for unidirectional fiber composites. J Appl Mech 1981;20:329–34.

[3] Matzenmiller A, Lubliner J, Taylor RL. A constitutive model for anisotropic damage in fiber composites. Mech Mater 1995;20:125–52.

[4] Camanho PP, Davila CG, De Moura MF. Numerical simulation of mixed-mode progressive delamination in composite materials. J Compos Mater 2003;37(16):1415–37.

[5] Ortiz M, Pandolfi A. Finite-deformation irreversible cohesive elements for three-dimensional crack-propagation analysis. Int J Numer Methods Eng 1999; 44:1267–82.

[6] Daniel IM, Ishai O. Engineering mechanics of composite materials. New York: Oxford; 1994.

[7] Crews JH, Reeder JR. A mixed-mode bending apparatus for delamination testing. NASA TM 100662; 1988.

[8] Naghipour P, Schneider J, Bartsch M, Hausmann J, Voggenreiter H. Fracture simulation of CFRP laminates in mixed mode bending. Eng Fract Mech 2009; 76:2821–33.

# 7 Fatigue and Fracture of Engine Materials

## 7.1 Fatigue crack propagation measurements on IN718 in the temperature and stress range of dynamic embrittlement

*K. Wackermann (LMW), U. Krupp (HS Osnabrück), H.-J. Christ ( LMW)*

Alloy 718 is a standard nickel-base alloy for high-temperature applications, e.g. as forged gas turbine discs or blades. At elevated temperatures alloy718 is prone to fast intergranular dwell-time cracking at high crack propagation rates da/dN. This kind of time-dependent cracking is governed by dynamic embrittlement, a failure mechanism that describes a combination of tensile-stress-assisted oxygen grain boundary diffusion leading to a time- and cycle-dependent loss of the grain boundary cohesion. Contrary to that, under vacuum or inert gas conditions crack propagation rates are slower and the respective fracture surfaces appear ductile and transcrystalline. The crack propagation rates do not depend exclusively on the surrounding atmosphere but also on the duration of the dwell time at maximum load in the fatigue cycle. Increasing dwell-time durations lead to faster crack propagation rates, Figure 7.1.

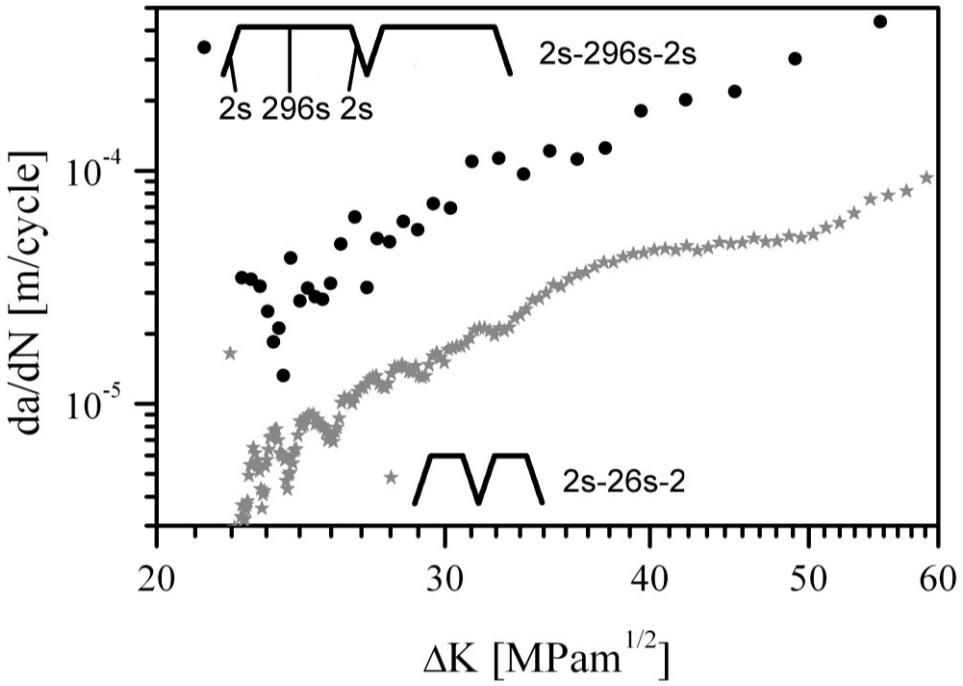


**Figure 7.1 Crack propagation rates on alloy718 at 650°C in laboratory air in dwell-time tests in stress-control for one load mode with 2s increase to maximum load, 296s at maximum load and 2s decrease to minimum load (2s-296s-2s) and one load mode 26s at maximum load (2s-26s-2s).**

Objective of this study is a better understanding of the intercrystalline cracking phenomenon "dynamic embrittlement". Of the utmost interest is the interaction of dwell-time and fatigue on the crack propagation and the correlation between the crack propagation rate with different stages of the loading cycle, namely the dwell-time and the fatigue load reversals between dwell-times. This shall be achieved by combined crack propagation measurements with (i) an alter-

nate current potential drop system (ACPD) and with (ii) a Questar far-field microscope. The far-field microscope allows the observation of the crack propagation on the surface of one side of a corner-crack specimen. In contrast, the ACPD system measures the bulk crack length.

So far, crack propagation test with different frequencies and dwell-times were performed on corner crack specimen with a quadratic cross section of 7mm, cf. Figure 7.1 and Figure 7.2. The tests reveal that the fatigue load reversals and the dynamic embrittlement during the dwell-time are interacting crack driving forces. Low ranges of the stress intensity factor (ΔK) or short dwell-times result in a fatigue-dominated crack propagation and a rather transcrystalline fracture morphology. High ΔK or long dwell-times result in a crack propagation dominated by the diffusion controlled dynamic embrittlement and an intercrystalline fracture morphology.

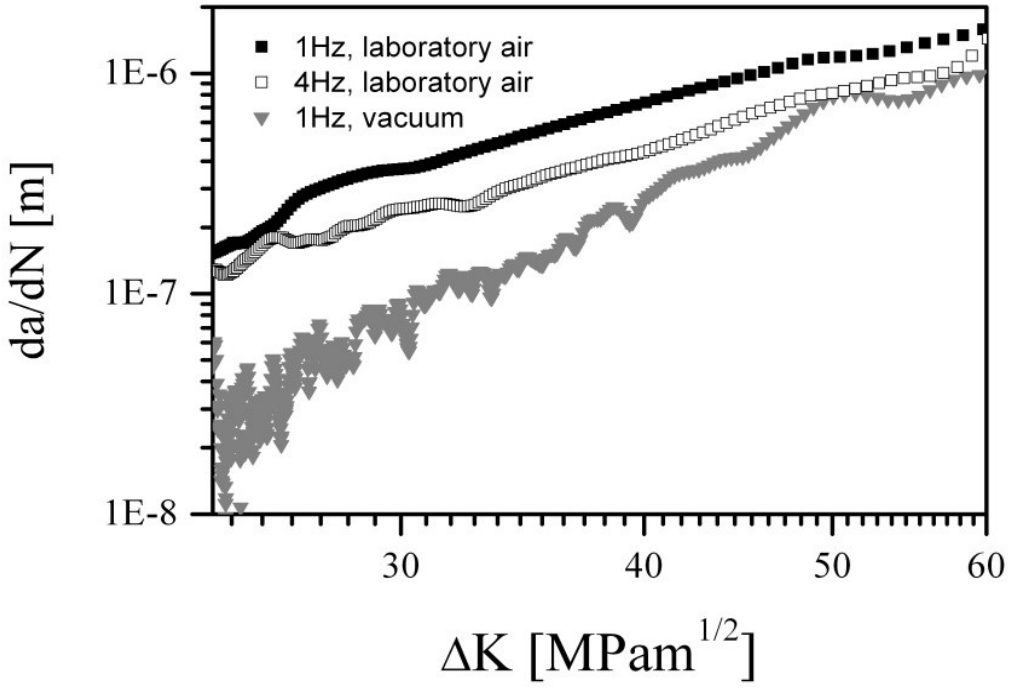


**Figure 7.2 Crack propagation rate for tests in vacuum and laboratory air in sinus loading at different frequencies.**

## 7.2 Enhancing the fatigue properties of the metastable β-Titanium alloy Ti 38-644 by obtaining a superior microstructure via Thermohydrogen Treatment (THT)

*V. Macin, P. Schmidt, H.-J. Christ (LMW)*

Excellent corrosion resistance, reasonable room temperature formability and very good fatigue endurance make the highly stabilized (solute-rich) β titanium alloys attractive materials for fatigue critical components in structural aerospace applications requiring high strength as well as low weight at the same time. In this context, the applicability range of β titanium alloys might be restricted due to their proneness to an inhomogeneous precipitation of the strengthening α phase within the β microstructure and the formation of soft α phase layers along the β grain boundaries ($\alpha_{GB}$ phase). The formation of precipitate-free zones (PFZ) and grain boundaries α

phase are known to be microstructural key features determining life of highly stabilized β titanium alloys since monotonic and cyclic plastic deformation are concentrated in these weak regions. Such microstructure phenomena control fatigue crack initiation as well as fatigue crack propagation with increasing yield strength of the material. This alloy class can be heat-treated to a broad range of strength to ductility ratios, whereby duplex aging consisting of the low and high temperature aging is despite of the complexity the best conventional heat treatment to establish a more homogeneous distribution of strengthening α precipitates.

Increasing demands for better performance of components and structures necessitate innovative routes of thermomechanical processing. In the present study hydrogen is used as a temporary alloying element within the heat treatment. It's referred to as Thermohydrogen Treatment (THT) and it facilitates the improvement of particular mechanical properties of the highly stabilized β titanium alloy Ti 38-644 (β-C) by means of microstructure modification. The β titanium alloys feature excellent characteristics concerning kinetics and thermo-dynamics of hydrogen sorption. The hydrogen induced phase plays an essential role in the successful implementation of THT.

According to Figure 7.3a, the THT strategy *hydride-induced alteration of dislocation arrangement* (HADA) contained five treatment steps: recrystallization, diffusion controlled hydrogenation, hydride formation, dehydrogenation and aging. Complete recrystallization for 30min at 920°C (1$^{nd}$ step) enabled the formation of (Ti, Zr)$_3$Si$_5$ particles, acting as precursors for the hydride formation and requirement of homogeneous distribution of the hydride phase. Subsequently β-C was hydrogenated to 0,6wt.-% H for 2hrs at 700°C (2$^{nd}$ step) leading to a slight hydride formation only at β grain boundaries (hydride seams). Interstitially dissolved hydrogen caused solid solution hardening with an increase in hardness from 290HV to 330HV. The formation of the hydride, referred to as the λ phase ($Ti_2ZrH_4$) and the δ phase ($TiH_2$) (see Figure 7.3b), by annealing for 2 hrs at 650°C (3$^{nd}$ step) was carried out by reducing the temperature below the solubility limit at 0,6at.-% H.

The volume effects associated with hydride formation led to local matrix deformation accompanied by accumulation and pile-up of dislocations. An enhanced kinetics of hydride nucleation reduces the annealing time to 2hrs or less being necessary to facilitate a homogeneous distribution of acicular and plate-type hydrides. The radial hydride precipitation initiating from silicides (see Figure 7.3c) led to a precipitation hardening resulting in a hardness to 360HV. In order to avoid hydrogen embrittlement, dehydrogenation was done by vacuum annealing for 45min at 780°C using Zr-foil as an auxiliary getter material to accelerate hydrogen release (4$^{nd}$ step). The hardness of 360HV after dehydrogenation indicated remaining strain hardening after the hydride dissolution and completely hydrogen release.

The THT strategy was completed by aging for 20hrs at 500°C (5$^{nd}$ step) leading to a precipitation of refined α particles homogeneously distributed without any formation of $\alpha_{GB}$ phase (see Figure 7.3d). A final hardness was obtained of more than 470HV based on precipitation hardening as well as hydride-induced deformation hardening. The reduction of the required aging time compared to the duplex-aging cycle indicates enhanced kinetics of α phase nucleation due to hydride-induced β crystal lattice distortion, which intensified the α precipitation during aging. Since the volume fraction of the hydride phase and the hydride particle distribution can be controlled by the THT parameters (particularly annealing time and temperature, dehydrogenation temperature), the size of the α phase precipitates and associated precipitation hardening can be adjusted.

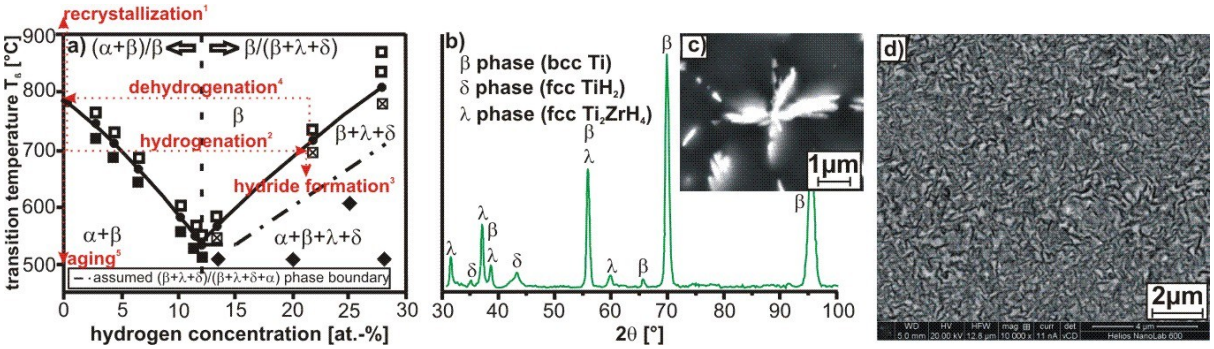


**Figure 7.3 a) THT strategy inscribed schematically in the phase diagram of β-C; b) X-ray diffraction patterns after hydride formation3; c) Hydride formation in β-C starting radially from silicides; d) Microstructure finally obtained in β-C after 5-step thermohydrogen treatment**.

## 7.3 High-Temperature Low Cycle Fatigue of the gamma alloy TNB-V2

*A. El-Chaikh, H.-J. Christ (LMW), T.K. Heckel (RR)*

In recent times, γ-TiAl-based alloys have found large-scale implementation as blade material into advanced aero engines, substituting heavy-weight nickel-based alloys. A remaining crucial issue is however to assess the material's maximum reliable fatigue performance under operating conditions (i.e. guaranteeing a minimum LCF life of 10,000 cycles). Investigations conducted at the authors' institution have revealed that the high-temperature low cycle fatigue behaviour of the advanced γ-TiAl-based alloy TNB-V2, containing 8 at.-% niobium, is rather modest at an applied total strain amplitude of $\Delta\varepsilon_t/2$= 0.7% under fully-reversed testing conditions. In the temperature field between 550°C and 850°C, fatigue life never exceeded 600 cycles. At this high $\Delta\varepsilon_t/2$ the temperature has no clear influence on the fatigue life of TNB-V2 (Figure 7.4a), since the damages were caused mainly by the high plastic strain amplitude leading to early initiation of cracks.

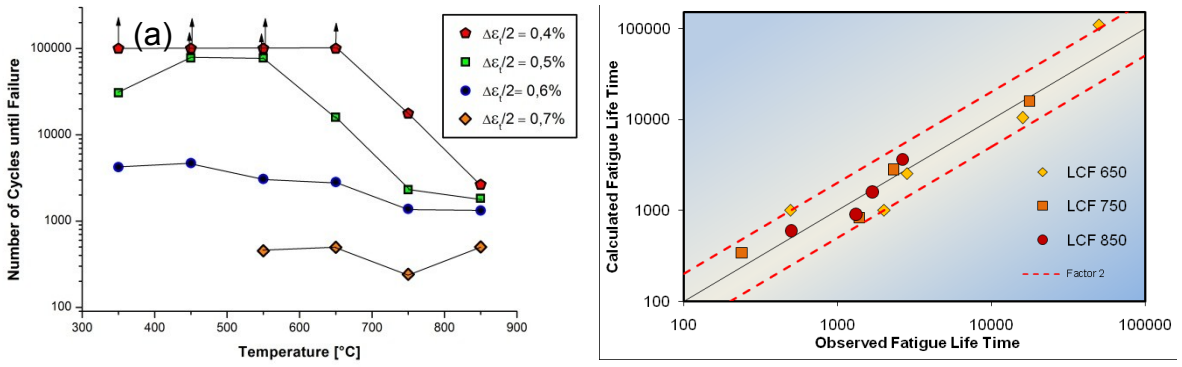


**Figure 7.4 a) cycles to failure, and b) calculated fatigue lives versus determined fatigue lives for tests performed at $\Delta\varepsilon_t/2$= 0.4%, 0.5%, 0.6% and 0.7%.**

At $\Delta\varepsilon_t/2$ less than 0.7% a reduction of life with rising temperature can be observed and is related to the effect of oxidation. At the lowest $\Delta\varepsilon_t/2$ (0.4%) failure occurs only at elevated temperatures (750°C and 850°C) showing clearly the effect of the environment on the fatigue life of TNB-V2.

The comparison of the fatigue lives at temperatures below the ductile-brittle transition temperature (DBTT which is 800°C for TNB-V2) shows that a small increase in the strain amplitude of only 0.1% reduces the life considerably.

A life prediction model for the fatigue life, based on the Basquin-Coffin-Manson law was applied to the results for TNB-V2 at all strain amplitudes. The number of cycles until failure can be calculated after determining the parameters of the Basquin-Coffin-Manson equation. Due to the acceptable amount of the plastic strain amplitude for LCF tests performed at temperatures above 650°C a suitable scatter band of 2 can be obtained after plotting the calculated number of cycles versus the observed number of cycles (Figure 7.4b) for the temperatures 650°C, 750°C and 850°C and all $\Delta\varepsilon_t/2$ (from 0.4% to 0.7%).

**Acknowledgement**

The financial support by Deutsche Forschungsgemeinschaft (DFG, grant No. CH 92/37-2) is gratefully acknowledged.

# 8 Non-Destructive Testing

## 8.1 Unimechanics: Discovering the Least Square Method Defects and Paradoxicalness

*Lev G. Gelimson (AICFS)*

In data processing, the least square method (LSM) [1] by Legendre and Gauss is practically the unique known one applicable to contradictory problems. But universal mathematics [2-5] has discovered that the LSM is based on the absolute error not invariant by equivalent transformations of a problem and loses any sense by possibly noncoinciding physical dimensions (units). The LSM simply mixes data without their adequately weighing, iterating, flexibility, and justification. The LSM paradoxically gives greater (even absolute) errors by smaller absolute values in approximation.

Universal mechanics [3] has additionally discovered further defects and paradoxicalness of the LSM. Consider its typical simplest approach. Minimizing the sum of the squared differences of the alone preselected coordinates (e.g., ordinates in a two-dimensional problem) of the graph of the desired approximation function and of every given data depends on this preselection, ignores the remaining coordinates, and provides no coordinate system rotation invariance and hence no objective sense of the result. Moreover, the LSM is correct by constant approximation or no data scatter only and gives systematic errors increasing together with data scatter and the deviation (namely declination) of an approximation from a constant.

Place the origin O of the coordinate system Oxy at the center of gravity of any planar data point set F mirror-symmetric with respect to Ox so that for the moments of inertia of F, $J_x = \int_F y^2 dF < J_y = \int_F x^2 dF$, $J_{xy} = \int_F xy dF = 0$. Fix initial Oxy as Ox'y' and rotate set F with Oxy about O by any angle α (Figure 8.1Figure 8.2). In Ox'y' with $x' = x \cos \alpha - y \sin \alpha$ , $y' = x \sin \alpha + y \cos \alpha$ , $c = \tan \alpha$ , fit F via the LSM line $y' = kx' = (\tan \beta)x'$:

$$_{x'}{}^2S(k) = \int_F (kx' - y')^2 dF = \min; \; d_{x'}{}^2S(k)/dk = 0; \; \int_F 2x'(kx' - y')dF = 0; \; k = \int_F x'y'dF / \int_F x'^2 dF;$$
$$\int_F x'y'dF = \sin \alpha \cos \alpha \int_F (x^2 - y^2)dF + (\cos^2 \alpha - \sin^2 \alpha) \int_F xydF = c(J_y - J_x)/(1 + c^2);$$
$$\int_F x'^2 dF = \cos^2 \alpha \int_F x^2 dF - 2\sin \alpha \cos \alpha \int_F xydF + \sin^2 \alpha \int_F y^2 dF = (J_x c^2 + J_y)/(1 + c^2);$$
$$k = c(J_y - J_x)/(J_x c^2 + J_y), \; k_{max} = 0.5(J_y - J_x)/(J_x J_y)^{1/2} \text{ at } c_{max} = (J_y/J_x)^{1/2}.$$

Nota bene: By increasing α from 0 over arctan $c_{max}$ to 90°, the LSM gives β increasing from 0 to arctan $k_{max}$ and then suddenly decreasing to 0, respectively. The LSM slope $k_{max}$ is about 0.34 and 0.89 whereas arctan $k_{max}$ is about 19.47° and 41.79° only, respectively. Distance quadrat theories and general theories of moments of inertia give correct results even by great data scatter, e.g. in aeronautical fatigue.

**Acknowledgements** to Anatolij Gelimson for our constructive discussions on coordinate system transformation invariances and his very useful remarks.

**References:**

[1] Encyclopaedia of Mathematics. Ed. Michiel Hazewinkel. Volumes 1 to 10. Supplements I to III. Kluwer Academic Publ., Dordrecht, 1987-2002

[2] Lev Gelimson. General Problem Theory. Abhandlungen der WIGB (Wissenschaftlichen Gesellschaft zu Berlin), 3 (2003), Berlin, 26-32

[3] Lev Gelimson. Elastic Mathematics. General Strength Theory. The "Collegium" All World Academy of Sciences Publishers, Munich, 2004

[4] Lev Gelimson. Providing Helicopter Fatigue Strength: Flight Conditions. In: Structural Integrity of Advanced Aircraft and Life Extension for Current Fleets – Lessons Learned in 50 Years After the Comet Accidents, Proceedings of the 23rd ICAF Symposium, Claudio Dalle Donne (Ed.), 2005, Hamburg, Vol. II, 405-416

[5] Lev Gelimson. Corrections and Generalizations of the Least Square Method. In: Review of Aeronautical Fatigue Investigations in Germany during the Period May 2007 to April 2009, Ed. Dr. Claudio Dalle Donne, Pascal Vermeer, CTO/IW/MS-2009-076 Technical Report, International Committee on Aeronautical Fatigue, ICAF 2009, EADS Innovation Works Germany, 2009, 59-60

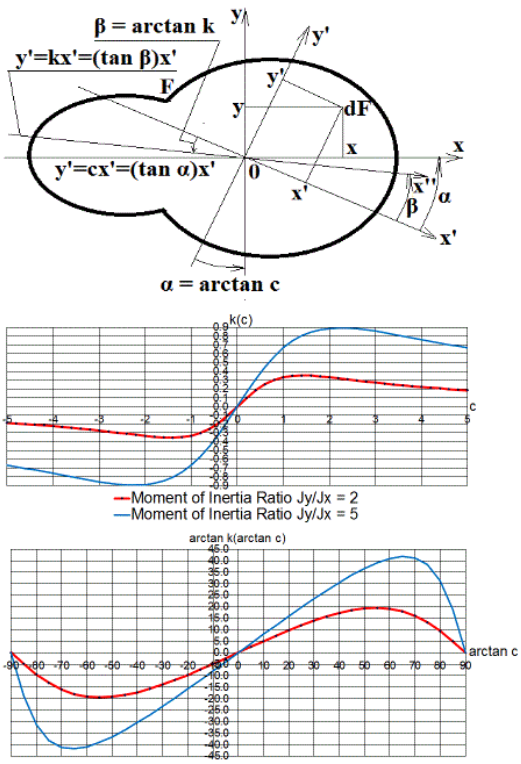


**Figure 8.1 The LSM Rotation Bounds**

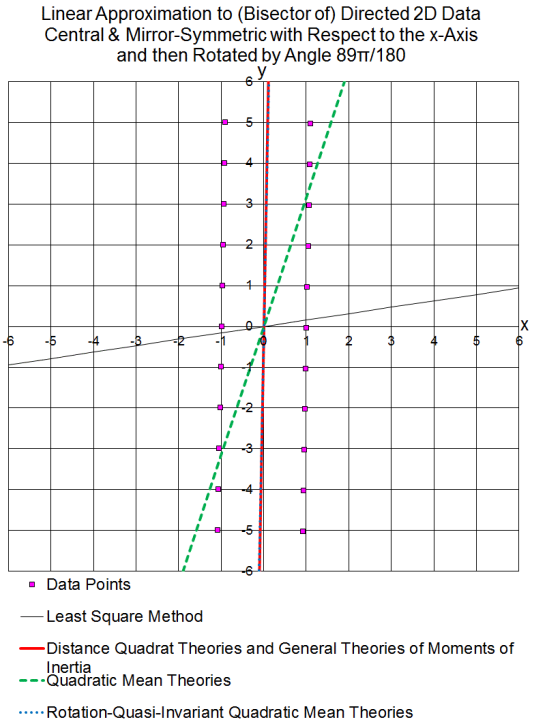


**Figure 8.2 Initially F ={(0,±1), (±1,±1), … , (±5,±1)} in the initial system Oxy**

## 8.2 Adjacent Sides and Corners Bisectors Theories in Universal Problem Solving Science

*Lev G. Gelimson (AICFS)*

The least square method (LSM) [1] by Legendre and Gauss is practically the unique known one applicable to contradictory (e.g. overdetermined) problems in data processing. Universal mathematics [2-5] discovered many principal LSM defects.

Adjacent sides bisectors theory (ASBT) uses coordinate system rotation invariance via data centralization and standardization. In a plane, take a finite overdetermined quantiset [2-5] of n (n > 2; $n \in N^+ = \{1, 2, ...\}$) linear equations with their quantities q(i)

$$_{q(i)}(a_j x + b_j y = c_j)\ (j = 1, 2, \ldots, n)\ (E_i)$$

and 2 unknown variables x and y with real numbers q(i) > 0, $a_j$ , $b_j$ , and $c_j$ . Number the polygon $P_1P_2...P_n$ vertices $_{p(1)}P_1$ , $_{p(2)}P_2$ , ... , $_{p(n)}P_n$ and bisectors $_{p(1)}B_1$ , $_{p(2)}B_2$ , ... , $_{p(n)}B_n$ (with multiplying the line quantities) in the clockwise or anticlockwise order to provide its convexity or the minimum number of nonconvex corners. If by n > 3 there is no inscribed circumference whose center is the best quasisolution, subsequently replace every convex vertex with the intersection of its bisector and the straight line segment connecting the both adjacent corners with conserving its quantity. Decrease the polygon with possibly reordering and determine its weighted center.
Adjacent corners bisectors theory (ACBT) also rotation-invariant keeps all the internal intersections of the bisectors of the adjacent corners with replacing each external intersection via the nearest intersection of the bisector of those bisectors with the polygon boundary. Determine the weighted center of the conserved intersections.

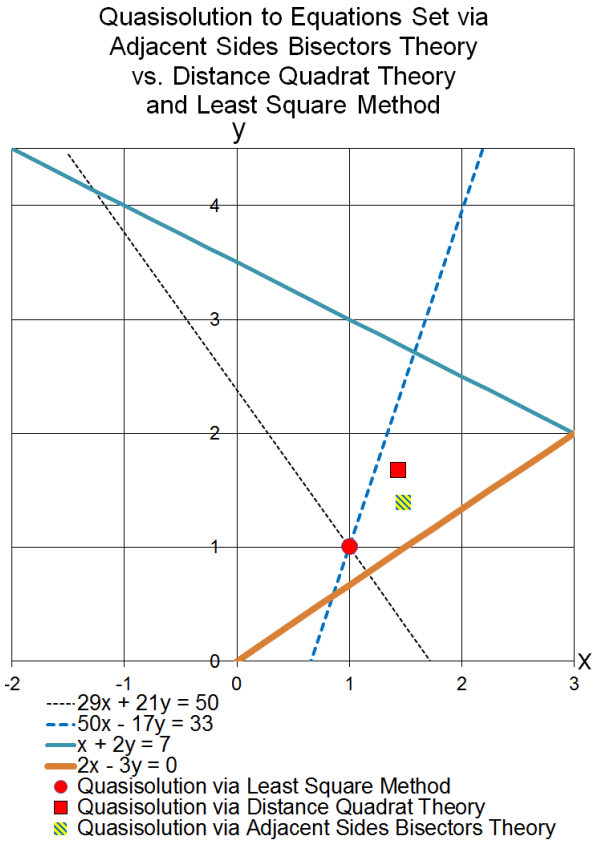


**Figure 8.3 Adjacent sides bisectors theory**

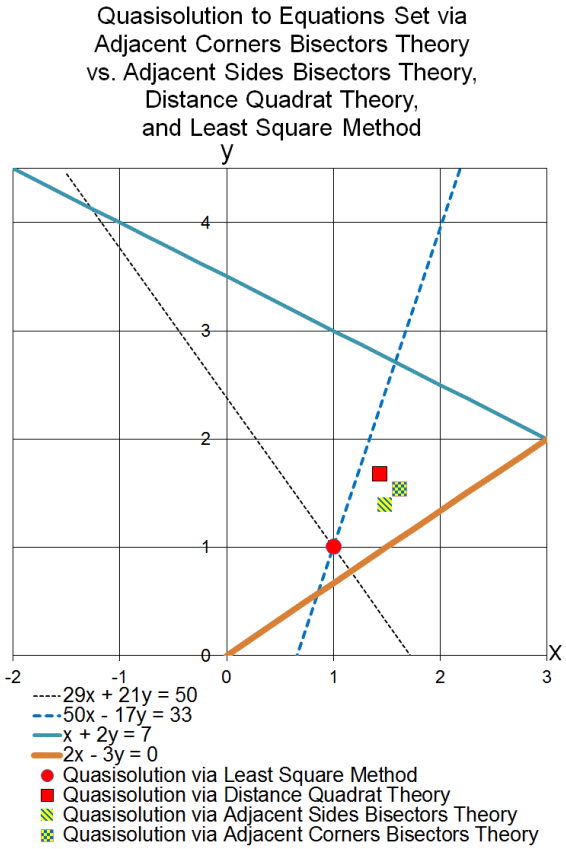


**Figure 8.4 Adjacent corners bisectors theory**

To solve equation set 29x + 21y = 50, 50x - 17y = 33, x+2y = 7, 2x-3y = 0 (Figure 8.3Figure 8.4), compare applying adjacent sides bisectors theory (ASBT) with one step only, adjacent corners bisectors theory (ACBT), distance quadrat theory (DQT) [2-4], and the least square method (LSM).

The LSM gives x ≈ 1.0023, y ≈ 1.0075 practically ignoring the last two equations with smaller factors (unlike ASBT, ACBT, and DQT).
Adjacent sides bisectors theory (ASBT) and adjacent corners bisectors theory (ACBT) providing simple explicit quasisolutions to even contradictory problems are very efficient by solving many urgent problems, e.g. in aeronautical fatigue.

**Acknowledgements** to Anatolij Gelimson for our constructive discussions on coordinate system transformation invariances and his very useful remarks.

**References:**

[1] Encyclopaedia of Mathematics. Ed. Michiel Hazewinkel. Volumes 1 to 10. Supplements I to III. Kluwer Academic Publ., Dordrecht, 1987-2002

[2] Lev Gelimson. General Problem Theory. Abhandlungen der WIGB (Wissenschaftlichen Gesellschaft zu Berlin), 3 (2003), Berlin, 26-32

[3] Lev Gelimson. Elastic Mathematics. General Strength Theory. The "Collegium" All World Academy of Sciences Publishers, Munich, 2004

[4] Lev Gelimson. Providing Helicopter Fatigue Strength: Flight Conditions. In: Structural Integrity of Advanced Aircraft and Life Extension for Current Fleets – Lessons Learned in 50 Years After the Comet Accidents, Proceedings of the 23rd ICAF Symposium, Claudio Dalle Donne (Ed.), 2005, Hamburg, Vol. II, 405-416

[5] Lev Gelimson. Corrections and Generalizations of the Least Square Method. In: Review of Aeronautical Fatigue Investigations in Germany during the Period May 2007 to April 2009, Ed. Dr. Claudio Dalle Donne, Pascal Vermeer, CTO/IW/MS-2009-076 Technical Report, International Committee on Aeronautical Fatigue, ICAF 2009, EADS Innovation Works Germany, 2009, 59-60

## 8.3 Opposite Sides and Corners Bisectors Theories in Universal Problem Solving Science

*Lev G. Gelimson (AICFS)*

Data processing is commonly based on the least square method (LSM) [1] by Legendre and Gauss practically the unique known one applicable to contradictory problems. Universal mathematics [2-5] discovered a lot of principal LSM defects.

Opposite sides bisectors theory (ASBT) uses coordinate system rotation invariance via data centralization and standardization. In a plane, take a finite overdetermined quantiset [2-5] of n (n > 2; $n \in N^+ = \{1, 2, ...\}$) linear equations with their quantities q(i)

$$_{q(i)}(a_jx + b_jy = c_j)\ (j = 1, 2, ... , n)\ (E_i)$$

and 2 unknown variables x and y with real numbers q(i) > 0, $a_j$ , $b_j$ , and $c_j$ . If n = 2m (even), then for any j = 1, 2, ... , m , consider m disordered sides pairs $P_jP_{j+1}$ and $P_{j+m}P_{j+1+m}$ of sides (edges) of this polygon as its opposite sides. For each pair, determine the set of all the bisectors equidistant from the two straight lines containing these sides and the intersection of the equidistant line(s) with the polygon area. Then determine the bisectors intersections and their weighted center (Figure 8.5). If n = 2m + 1 (odd), then for any i = 1, 2, ... , 2m + 1, similarly consider both quasiopposite pairs ($P_iP_{i+1}$ , $P_{i+m}P_{i+m+1}$) and ($P_iP_{i+1}$ , $P_{i+m+1}P_{i+m+2}$).

Opposite corners bisectors theory (OCBT) also rotation-invariant deals with disordered opposite corners pairs ($P_j$ , $P_{j+m}$) (j = 1, 2, ... , m by n = 2m) or both quasiopposite ($P_i$ , $P_{i+m}$) and ($P_i$ , $P_{i+m+1}$) (i = 1, 2, ... , 2m + 1 by n = 2m + 1) and their bisectors intersections. Then determine their weighted center (Figure 8.6).

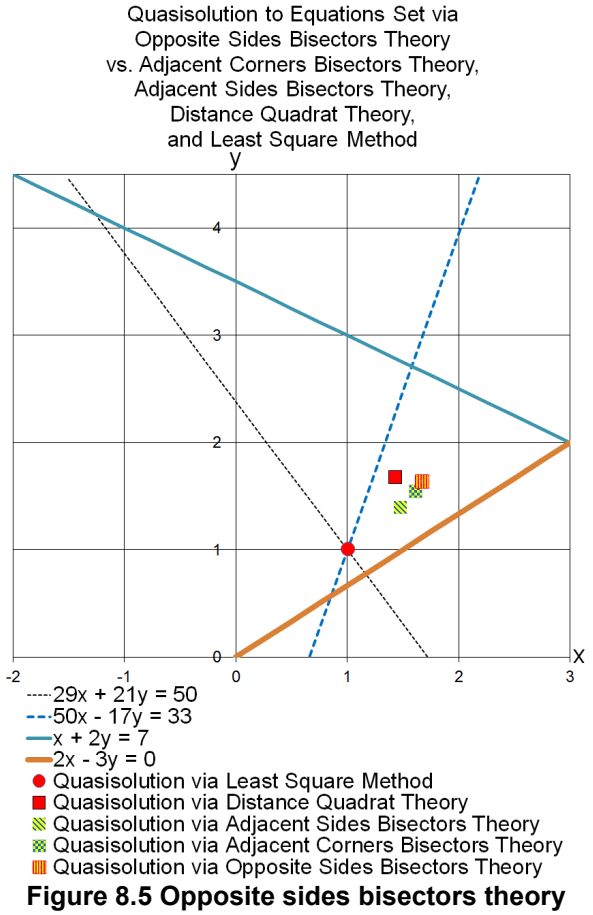


**Figure 8.5 Opposite sides bisectors theory**

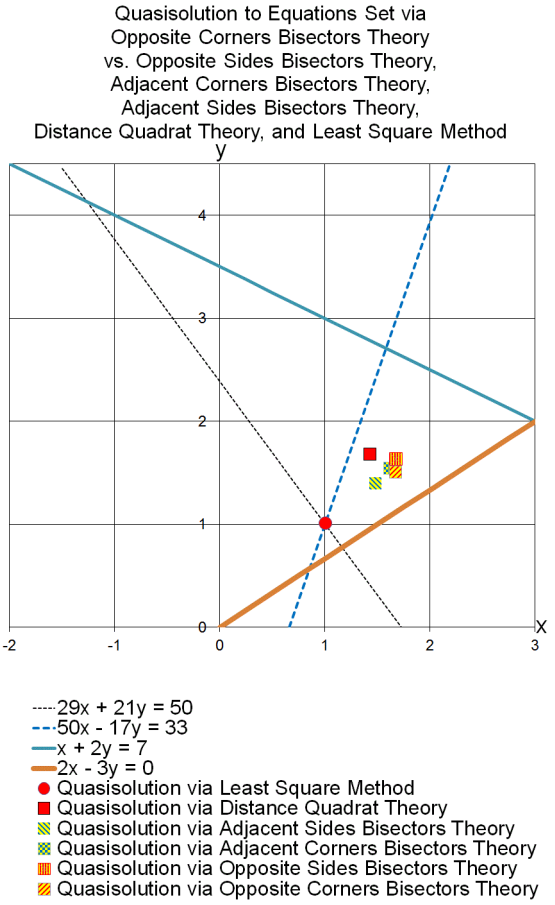


**Figure 8.6 Opposite corners bisectors theory**

Compare applying OSBT, OCBT, adjacent sides bisectors theory (ASBT) with one step only, adjacent corners bisectors theory (ACBT), distance quadrat theory (DQT) [2-4], and the least square method (LSM) to solve this test equation set 29x + 21y = 50, 50x - 17y = 33, x + 2y = 7, 2x - 3y = 0 (see Figure 8.5Figure 8.6). The LSM almost ignores the last two equations with smaller factors (unlike OSBT, OCBT, ASBT, ACBT, DQT).
Opposite sides bisectors theory (OSBT) and opposite corners bisectors theory (OCBT) providing simple explicit quasisolutions to even contradictory problems are very efficient by solving many urgent problems, e.g. in aeronautical fatigue.

**Acknowledgements** to Anatolij Gelimson for our constructive discussions on coordinate system transformation invariances and his very useful remarks.

**References:**

[1] Encyclopaedia of Mathematics. Ed. Michiel Hazewinkel. Volumes 1 to 10. Supplements I to III. Kluwer Academic Publ., Dordrecht, 1987-2002

[2] Lev Gelimson. General Problem Theory. Abhandlungen der WIGB (Wissenschaftlichen Gesellschaft zu Berlin), 3 (2003), Berlin, 26-32

[3] Lev Gelimson. Elastic Mathematics. General Strength Theory. The "Collegium" All World Academy of Sciences Publishers, Munich, 2004

[4] Lev Gelimson. Providing Helicopter Fatigue Strength: Flight Conditions. In: Structural Integrity of Advanced Aircraft and Life Extension for Current Fleets – Lessons Learned in 50 Years After the Comet Accidents, Proceedings of the 23rd ICAF Symposium, Claudio Dalle Donne (Ed.), 2005, Hamburg, Vol. II, 405-416

[5] Lev Gelimson. Corrections and Generalizations of the Least Square Method. In: Review of Aeronautical Fatigue Investigations in Germany during the Period May 2007 to April 2009, Ed. Dr. Claudio Dalle Donne, Pascal Vermeer, CTO/IW/MS-2009-076 Technical Report, International Committee on Aeronautical Fatigue, ICAF 2009, EADS Innovation Works Germany, 2009, 59-60

## 8.4 Equidistance and Subjoining Equations Theories in Universal Problem Solving Science

*Lev G. Gelimson (AICFS)*

For data processing, the least square method (LSM) [1] by Legendre and Gauss practically the unique known one applicable to contradictory problems seems to be irreplaceable. Universal mathematics [2-5] discovered: the LSM has principal defects.

Equidistance theory (EDT) stepwise excludes equations and then regards them. Determine all the n intersections of the bisectors of the adjacent corners of the linear equation set polygon. For intersection $R_i$ , determine its distance $d_i$ from the polygon side $E_i$ connecting the both corresponding adjacent corners of the polygon, the minimum distance $d_{min}$ , and all the polygon sides providing $d_{min}$. Move each polygon edge to the interior by $d_{min}$ whereas the initial and the end positions of this polygon side are the opposite sides of the corresponding movement rectangle. Reduce the polygon sides number to obtain a triangle. Determine its incenter. Give it the sum quantity. For each remaining edge, determine the base (with the initial side quantity) of the perpendicular from this center to the straight line including the fixed end position of this initial polygon side. Determine the weighted center of these points.

Subjoining equations theory (SJET) also rotation-invariant begins with 3 equations whose straight lines intersections are the corners of a triangle including the given equations polygon and then stepwise subjoins the remaining equations (Figure 8.7Figure 8.8).

Compare applying EDT, SJET, opposite sides bisectors theory (OSBT), opposite corners bisectors theory (OCBT), adjacent sides bisectors theory (ASBT), adjacent corners bisectors theory (ACBT) with one step only, distance quadrat theory (DQT) [2-4], and the least square method (LSM) to solving the test equation set 29x + 21y = 50, 50x - 17y = 33, x + 2y = 7, 2x - 3y = 0. The LSM ignores the last two equations with smaller factors (unlike EDT, SJET, OSBT, OCBT, ASBT, ACBT, and DQT).

EDT and SJET providing simple explicit quasisolutions to contradictory problems are very efficient by solving many urgent problems, e.g. in aeronautical fatigue.

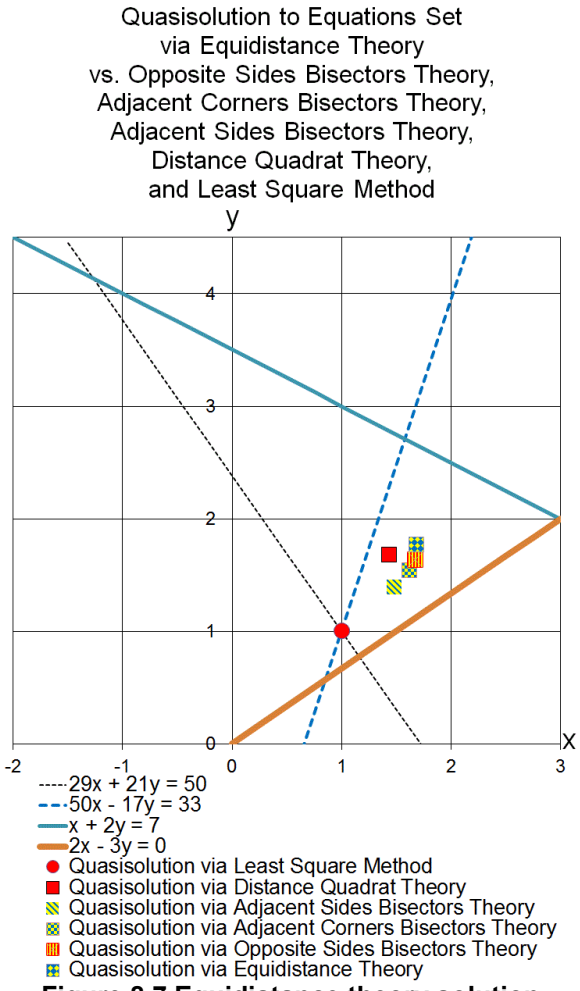


**Figure 8.7 Equidistance theory solution**

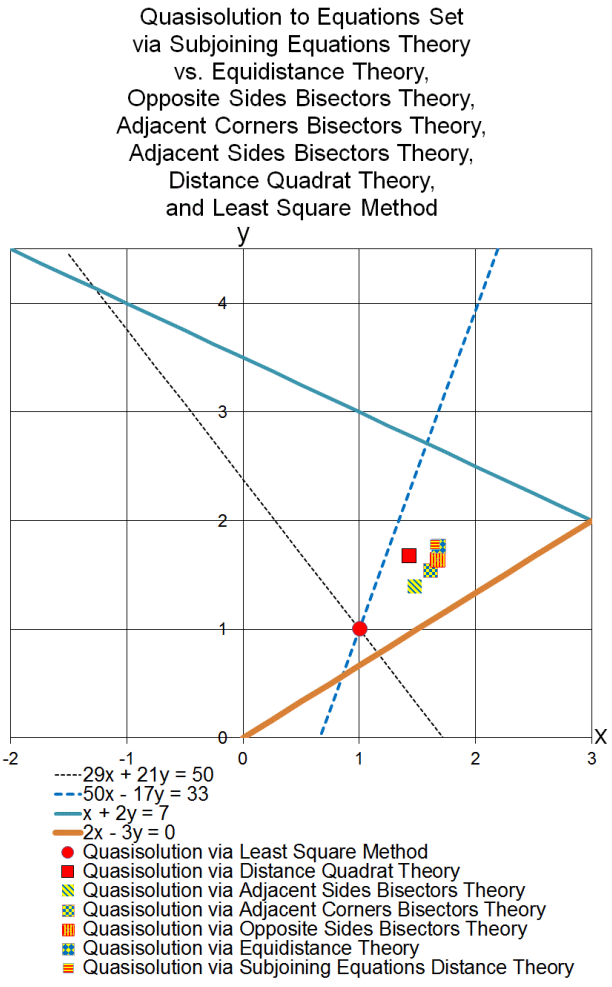


**Figure 8.8 Subjoining equations theory**

**Acknowledgements** to Anatolij Gelimson for our constructive discussions on coordinate system transformation invariances and his very useful remarks.

**References:**

[1] Encyclopaedia of Mathematics. Ed. Michiel Hazewinkel. Volumes 1 to 10. Supplements I to III. Kluwer Academic Publ., Dordrecht, 1987-2002

[2] Lev Gelimson. General Problem Theory. Abhandlungen der WIGB (Wissenschaftlichen Gesellschaft zu Berlin), 3 (2003), Berlin, 26-32

[3] Lev Gelimson. Elastic Mathematics. General Strength Theory. The "Collegium" All World Academy of Sciences Publishers, Munich, 2004

[4] Lev Gelimson. Providing Helicopter Fatigue Strength: Flight Conditions. In: Structural Integrity of Advanced Aircraft and Life Extension for Current Fleets – Lessons Learned in 50 Years After the Comet Accidents, Proceedings of the 23rd ICAF Symposium, Claudio Dalle Donne (Ed.), 2005, Hamburg, Vol. II, 405-416

[5] Lev Gelimson. Corrections and Generalizations of the Least Square Method. In: Review of Aeronautical Fatigue Investigations in Germany during the Period May 2007 to April 2009, Ed. Dr. Claudio Dalle Donne, Pascal Vermeer, CTO/IW/MS-2009-076 Technical Report, In-

ternational Committee on Aeronautical Fatigue, ICAF 2009, EADS Innovation Works Germany, 2009, 59-60

## 8.5 Distance and Unierror Power Theories in Universal Problem Solving Science

*Lev G. Gelimson (AICFS)*

The least square method (LSM) [1] by Legendre and Gauss is practically the unique known one applicable to contradictory (e.g. overdetermined) problems in data processing. Universal mathematics [2-5] has discovered many principal LSM defects.

Distance power theories (DPT) (with any power exponent $t > 1$) use coordinate system rotation invariance via data centralization and standardization, e.g. by a finite overdetermined quantiset [2-5] of $n$ ($n > m$; $m , n \in N^+ = \{1, 2, ...\}$) linear equations

$$_{q(j)}(\Sigma_{i=1}^{m} a'_{ij}x_i + c'_j = 0)\ (j = 1, 2, ... , n)\ (L'_j) \text{ to } _{q(j)}(\Sigma_{i=1}^{m} a_{ij}x_i + c_j = 0)\ (L_j)$$

with their own positive number quantities $q(i)$, $m$ pure number unknown variables $x'_i$ ($i = 1, 2, ... , m$), and any given real numbers $a'_{ij}$ and $c'_j$ in the $m$-dimensional "space" via dividing $(L'j)$ by $(\Sigma_{i=1}^{m} a'^{2}_{ij})^{1/2}$. The distance between the $j$th $m$-1-dimensional "plane" and point $(x_1 , x_2 , ... , x_m)$ is $d_j = |\Sigma_{i=1}^{m} a'_{ij}x_i + c'_j|/(\Sigma_{i=1}^{m} a'^{2}_{ij})^{1/2}$. Then minimize $^tS(x_1 , x_2 , ... , x_m) = \Sigma_{j=1}^{n} q(j)|e_j|^t = \Sigma_{j=1}^{n} q(j)\ |\Sigma_{i=1}^{m} a_{ij}x_i + c_j|^t$ via intelligent iteration.

Linear (LEPT) and square (SEPT) unierror power theories are also based on intelligent iteration, as well as on linear and square unierrors [2-5] of $(L_j)$

$$^1E_j=|\Sigma_{k=1}^{m}a'_{kj}x_k-c'_j|/(\Sigma_{k=1}^{m}|a'_{kj}x_k|+|c'_j|)^2,\ ^2E_j=|\Sigma_{k=1}^{m}a'_{kj}x_k-c'_j|/[(m+1)(\Sigma_{k=1}^{m} a'^{2}_{kj}x_k^2 + c'^{2}_j)]^{1/2}.$$

To solve equation set $29x + 21y = 50$, $50x - 17y = 33$, $x+2y = 7$, $2x-3y = 0$ (Figure 8.9Figure 8.10), compare applying unierror biquadrat theories (EBQT), distance biquadrat theory (DBQT), biquadrat theory (BQT), unierror quadrat theories (EQT), distance quadrat theory (DQT) [2-5], and the least square method (LSM) [1]. The LSM ignores the last two equations with smaller factors (unlike EBQT, DBQT, BQT, EQT, and DQT). Both linear (LEQT) and square (SEQT) unierror quadrat theories give very near results, and we have shown the results obtained via linear unierror quadrat theory only. Increasing the power from 2 to 4 provides very substantially improving sensitivity.

Distance power theories (DPT), as well as linear (LEPT) and square (SEPT) unierror power theories providing simple explicit quasisolutions to contradictory problems are very efficient in solving many urgent problems, e.g. in aeronautical fatigue.

**Acknowledgements** to Anatolij Gelimson for our constructive discussions on coordinate system transformation invariances and his very useful remarks.

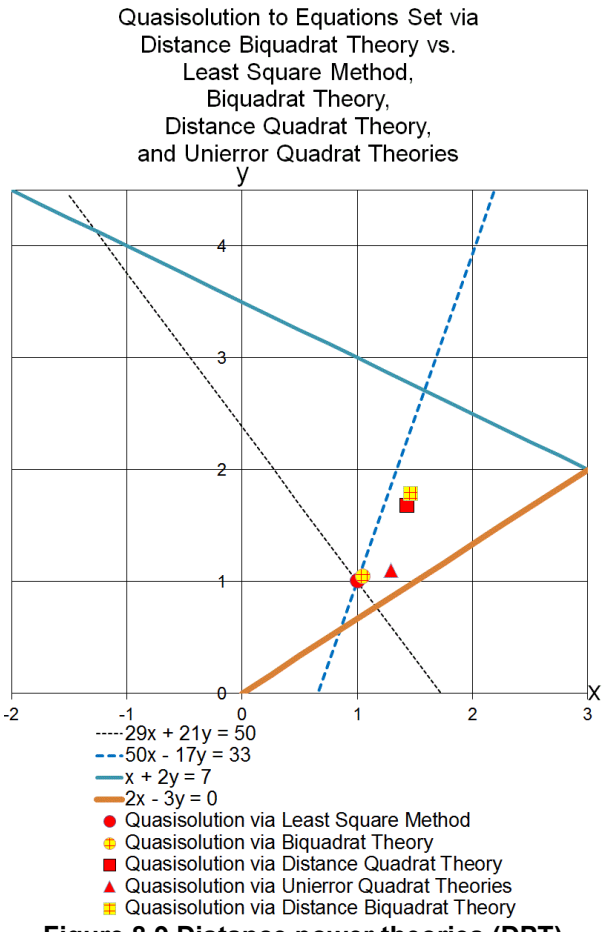


**Figure 8.9 Distance power theories (DPT)**

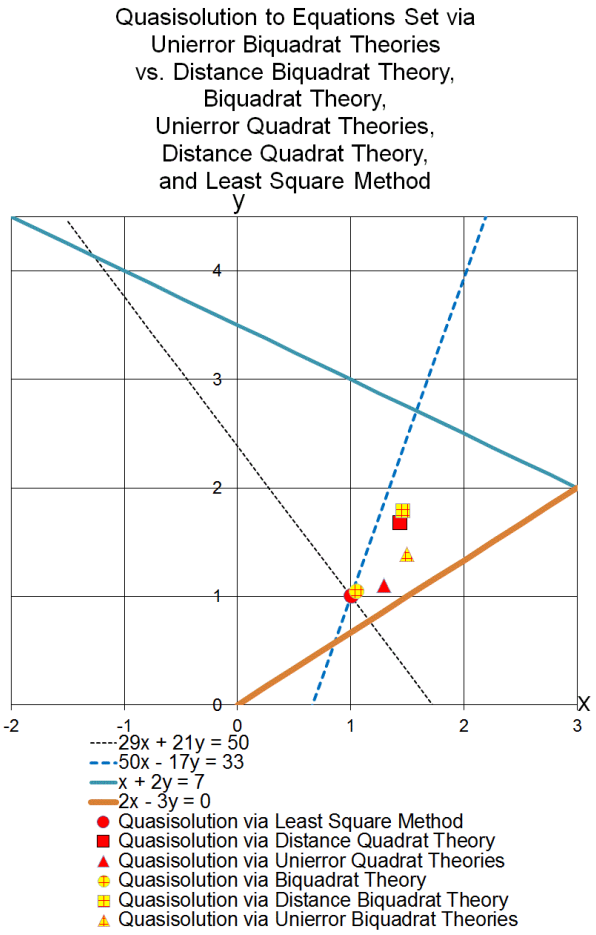


**Figure 8.10 Unierror power theories**

**References:**

[1] Encyclopaedia of Mathematics. Ed. Michiel Hazewinkel. Volumes 1 to 10. Supplements I to III. Kluwer Academic Publ., Dordrecht, 1987-2002

[2] Lev Gelimson. General Problem Theory. Abhandlungen der WIGB (Wissenschaftlichen Gesellschaft zu Berlin), 3 (2003), Berlin, 26-32

[3] Lev Gelimson. Elastic Mathematics. General Strength Theory. The "Collegium" All World Academy of Sciences Publishers, Munich, 2004

[4] Lev Gelimson. Providing Helicopter Fatigue Strength: Flight Conditions. In: Structural Integrity of Advanced Aircraft and Life Extension for Current Fleets – Lessons Learned in 50 Years After the Comet Accidents, Proceedings of the 23rd ICAF Symposium, Claudio Dalle Donne (Ed.), 2005, Hamburg, Vol. II, 405-416

[5] Lev Gelimson. Corrections and Generalizations of the Least Square Method. In: Review of Aeronautical Fatigue Investigations in Germany during the Period May 2007 to April 2009, Ed. Dr. Claudio Dalle Donne, Pascal Vermeer, CTO/IW/MS-2009-076 Technical Report, International Committee on Aeronautical Fatigue, ICAF 2009, EADS Innovation Works Germany, 2009, 59-60